Development and application of a new TILLING resource for the studies of sexual reproduction in *Arabidopsis thaliana*

（シロイヌナズナにおける有性生殖機構研究のための新たな TILLING 用リソースの作製とその適用）

Lai Kok Song

Nara Institute of Science and Technology

Graduate School of Biological Sciences

Intercellular Communications Laboratory (Professor Seiji Takayama)

2012/11/07

ABSTRACT

TILLING (targeting induced local lesions in genomes) is a reverse genetic method that can be employed to generate allelic series of induced mutations in targeted genes for functional analyses. To date, TILLING resources in *Arabidopsis thaliana* are only available in Columbia and Landsberg *erecta* accessions. Here, I extended the *Arabidopsis* TILLING resources by developing a new population of ethyl methanesulfonate (EMS)-induced mutant lines in another commonly used *A. thaliana* accession C24. The C24 accession is distinguished from other familial accessions in several physiological responses (e.g. stress tolerance, pathogen resistance) and the transgenic C24 with *S-locus* genes (*SRK/SP11*) exhibits stable self-incompatible (SI) phenotype, suggesting serving as a good model for understanding SI signalling.

A permanent collection of 3,509 independent EMS mutagenized M_2 lines was developed in *A. thaliana* accession C24, and designated the C24TILL collection. Querying the C24TILL collection for mutations in five selected genes expected to be involved in sexual reproduction process. A total of 86 mutations, comprising 63.9% missense, 25.6% sense, 1.2% nonsense and 9.3% intronic mutations were successfully identified. Consistent with the propensity of EMS to induce guanine alkylation, 97.6% of the observed mutations were G/C to A/T transitions. Based on the mutations identified in the five selected genes, the overall mutation density in the C24TILL collection was estimated to be 1/433 kb. Mutations in four selected genes namely *DUO1*, *APK1b*, *PKA*, and *EXO70C2* were evaluated from a functional standpoint.

Because *DUO1* is an essential gene for sperm cell speciation, a homozygous mutant line has never been obtained. Application of TILLING screen in the C24TILL collection identified a truncation *DUO1* mutation leading to a deficiency in

sperm cell differentiation. By contrast, two homozygous missense lines exhibit normal sperm cell specification indistinguishable from wild-type. Although attempt at obtaining homozygous *duo1* mutant with partial loss of function was unsuccessful, this study demonstrates that array of mutations can be identified for target genes from the established C24TILL collection.

Next, I focused on *APK1b* and *PKA* genes. The *APK1b* was previously identified as an *Arabidopsis* ortholog of *MLPK* shown to be involved in *Brassica* SI signalling. Meanwhile, *PKA* was a putative ortholog of *BrPKA*, which was identified from the yeast two-hybrid screening to search for the MLPK interactor. TILLING screen of C24TILL collection identified 3 and 7 missense mutations for *APK1b* and *PKA* respectively. Introgression of these missense mutations into the *SRK*-expressing C24 line did not change its self-incompatible phenotype (i.e. rejection of *SP11*-expressing pollen). As I could not judge the involvement of *APK1b* and *PKA* in SI signalling without obtaining truncation (nonsense) mutation, I also performed transformation experiments. Suppression of *APK1b* and *PKA* stigma's transcripts or overexpression of a non-functional kinase domain of APK1b neither abolishes nor weakens SI response in transgenic *Arabidopsis*, suggesting the non-functional role of these candidate genes in SI signalling.

Using the TILLING approach, I next analyzed the biological function of EXO70C2, a subunit of the exocyts complex shown to be predominantly expressed in pollen. TILLING screen identified *exo70c2* mutants with defect in pollen development and reduction in fertility. The *exo70c2* mutant pollen grains are aborted with abnormal morphology. Detail analysis showed that *EXO70C2* is localized to the cytoplasm and preferentially expressed in pollen. *In situ* hybridization further indicates that *EXO70C2* is specifically expressed in pollen and tapetal cells during

pollen development. My data suggest that, EXO70C2 is essential for *Arabidopsis* pollen development.

In conclusions, I have established a new reverse genetic tool for *A. thaliana* accession C24 by generating an EMS mutagenized population, the C24TILL collection, for use in combination with the TILLING screening method. The development of the C24TILL collection described here represents the third *A. thaliana* TILLING resource to date. TILLING for selected genes from this new collection successfully identified allelic series of induced point mutations which were then useful in functional genomics studies. The established C24TILL collection will serve to complement existing reverse genetic tools and provide a valuable resource to better understand the sexual reproduction process including SI mechanisms and other gene functions in *Arabidopsis*.

Table of contents

Page

Chapter 2: Functional characterization of *APK1b* and *PKA* in self-incompatible signalling of *Arabidopsis thaliana* accession C24

Chapter 3: Functional characterization of *EXO70C2* in pollen development

Chapter 1

Establishment of TILLING resource for *Arabidopsis thaliana* accession C24

1-1. Introduction

Many reverse genetic resources have been developed for functional genetic studies. Because site-directed mutagenesis is not effective in plants, random mutagenesis approaches, including insertional (Wisman et al. 1998; Alonso et al. 2003), chemical (McCallum et al. 2000) and fast neutron mutagenesis (Li et al. 2001), have been used to establish reverse genetic platforms. In *Arabidopsis*, insertional mutagenic techniques using T-DNA or transposons have become popular tools for functional genomics. However, insertional mutagenesis often leads to complete gene knockouts, making it difficult to associate nuanced phenotypes with essential genes (Jander et al. 2002). Similarly, radiation mutagenesis, *e.g.*, using fast neutrons, often induces large genomic deletions that affect multiple genes, again making associations with nuanced phenotypes difficult as well as obscuring the function of individual genes (Li et al. 2001). By contrast, classical chemical mutagenesis using a mutagen such as ethyl methanesulfonate (EMS) induces an array of point mutations with differing affects on gene function. Such allelic series are desirable because they generate a wide repertoire of mutant phenotypes covering a range of severity, which provides more insight into a gene's function. Moreover, individual plants carrying point mutations can be identified easily through a powerful technique called TILLING (targeting induced local lesions in genomes).

TILLING is a reverse genetic method that takes advantage of classical mutagenesis, sequence databases, and high-throughput PCR-based screening for

point mutations in a chosen sequence (Henikoff et al. 2004). The key advantage of TILLING over competing methods is that it can be applied to any plant species, regardless of ploidy, genome size, or genetic background (Kurowska et al. 2011). TILLING extends genomic resources, particularly in organisms lacking reverse genetic tools, where mutants with a range of phenotypic severity are highly desirable. Since its inception, TILLING has been applied to various organisms including *Cucumis melo* L. (González et al. 2011), *Solanum lycopersium* (Minioa et al. 2010), *Brassica napus* (Wang et al. 2008, Harloff et al. 2012), *Brassica oleracea* (Himelblau et al. 2009), *Brassica rapa* (Stephenson et al. 2010) *Lotus japonicus* (Perry et al. 2009), *Zea mays* (Till et al. 2004), *Oryza sativa* (Till et al. 2007), *Drosophila* (Winkler et al. 2005), and zebrafish (Wienholds et al. 2003).

To date, *Arabidopsis* TILLING resources are only available in accessions Columbia (Col-0) (Greene et al. 2003) and Landsberg *erecta* (L*er*) (Martín et al. 2009). Reverse genetic tools for many commonly used *Arabidopsis* accessions are still limited, in particular accession C24, which is genetically distinct from accession Col-0 (Barth et al. 2002; Törjek et al. 2003). C24 is distinguished physiologically from other familial accessions in terms of drought (Bechtold et al. 2010), ozone (Borshe et al. 2010), and frost tolerance (Rohde et al. 2004), and enhanced basal resistance to pathogens (Bechtold et al. 2010). Furthermore, the transgenic line of accession C24 with *A. lyrata S*-locus genes exhibited a robust and stable self-incompatible (SI) phenotype (Rea et al. 2010), which serves as a useful model for understanding SI signalling. In addition, a large portion of its genomic sequence is available (Schneeberger et al. 2011), making accession C24 an excellent alternative tool for plant research. However, the use of *A. thaliana* accession C24 has been hampered due to constrained reverse genetic resources. Therefore, the current work establishing a reverse genetic platform in accession C24 represents a major advance for functional genomics studies in plants.

In this study, I aimed to extend reverse genomic tools in *Arabidopsis* by establishing a new TILLING resource, the C24TILL collection, in the commonly used accession C24. Five candidate genes were selected for TILLING to evaluate the quality and test the robustness of the C24TILL collection in providing array of mutations. As a proof of principle, functional genetic analysis was performed on mutations in four selected genes. The established C24TILL collection will enable deeper functional genetic studies, especially for researchers aiming to understand novel gene functions in the unique C24 genetic background.

1-2. Materials and methods

1-2-1 EMS mutagenesis and establishment of a mutant population

Different concentrations of EMS (10, 25, 30 and 40 mM) were applied to the seeds of *A. thaliana* C24 accession for 15 h in 50 ml vials (~1,000 seeds) at room temperature (RT). After washing, approximately 600 treated seeds were sown in pots. The rate of mutagenesis achieved at different EMS concentrations was quantified based on seed germination rate and the percentage of albino chimera seedlings. For the production of C24TILL, an EMS concentration of 25 mM was used to mutagenize a batch of ~8,000 seeds for 15 h at RT before washing with distilled water. Seeds were sown in pots and individual seedlings were grown in Arasystem trays (Betatech, Gent, Belgium) to generate the M_1 population. From each individual M_1 plant, four M_2 offspring were grown and a single fertile M_2 plant was selected. In all, 3,509 individual M_2 plants were maintained. Genomic DNA and seed stocks were collected from these plants.

1-2-2 DNA extraction and pooling

Genomic DNA was extracted from the leaves of M_2 plants using a DNAeasy 96 Plant Kit (QIAGEN, USA) according to the manufacturer's protocol. Genomic DNA samples were quantified, diluted, and normalized to 1 ng/µl in 20% TE (10 mM Tris, 1 mM EDTA) solution. Samples were stored at -80°C. Using a one-dimensional pooling strategy as previously described (Martín et al. 2009), diluted genomic DNA (1 ng/µl) was pooled 8-fold. Pooled genomic DNA was stored at -20°C for use in the subsequent TILLING screen.

1-2-3 TILLING

Point mutations in targeted fragments were detected using the previously developed TILLING procedure (Till et al. 2006) with slight modifications. Each nested PCR reaction was performed in a 12.5 µl volume consisting of 1x PCR buffer (Takara, Shiga, Japan), 0.2 mM dNTPs, 2 U ExTaq polymerase (Takara, Shiga, Japan), 10 pmol forward and reverse unlabeled gene specific primers for the 1st PCR or 10 pmol forward (6 FAM-labeled) and reverse (VIC-labeled) common primers for the 2nd PCR, 5 µl of 0.5 ng/µl pooled genomic DNA for the 1st PCR or 1.0 µl of 1st PCR product for 2nd PCR and sterile H_2O. The reaction was performed using a 96-well thermal cycler (Astech, Kyoto, Japan) programmed with the following conditions: 1) 94°C for 3 minutes; 2) 15 (1st PCR) or 25 cycles (2nd PCR) of 94°C for 30 seconds, T_m-2°C for 30 seconds, and 72°C for 90 seconds; 3) and a final extension at 72°C for 7 minutes. The final PCR products were heated at 95°C for 10 minutes and slowly cooled (95°C ramping to 85°C at -2°C/second, then 85°C ramping to 25°C at -0.1°C/second) to generate heteroduplex PCR products. Five µl of the PCR reaction was treated with CEL 1 SURVEYOR nuclease (Transgenomic, Omaha, NE) and incubated at 45°C for 15 minutes. Then, 5 µl of 150 mM EDTA was added. The CEL

1-treated samples were cleaned through Sephadex G-50 resin (Amersham Pharmacia Biotech, Little Chalfont, UK) packed in 96-well Multiscreen-HV filter plates (Millipore, Billerica, MA). Next, the samples were mixed with 9.9 µl of HIDI Formamide and 0.1 µl of MapMarker® 1000 size standard (BioVentures, Murfreesboro, TN). The samples were heated at 95°C for 3 minutes before loading onto an ABI 3730xl (96-capillary) sequencer. Data were analysed using GENEMAPPER 4.0 fragment analysis software (ABI, Carlsbad, CA) and confirmed by DNA sequencing. Primers are listed in Supplemental Table 1.

1-2-4 Characterization of *duo1* mutant phenotype

Seeds from *duo1* TILLING mutants were stratified for 2 days at 4°C and plants were grown in soil in a growth chamber at 21°C and 60% relative humidity with a 16 h day/8 h night cycle. Genomic DNA was extracted from the leaves of the plants using a DNeasy Plant Mini Kit (QIAGEN, USA) according to the manufacturer's protocol. Genomic PCR was performed using *DUO1*-specific primers (Supplemental Table 1) and sequencing was carried out to confirm the presence of mutations. Pollen grains from mature flowers were transferred to a microcentrifuge tube containing 200 µl DAPI staining solution (0.1 M sodium phosphate, pH 7.5; 1 mM EDTA; 0.1 % Triton X-100; 0.4 µg/ml DAPI) and briefly mixed. The stained pollen was then transferred to a microscope slide and observed under a Zeiss Axioplan fluorescence microscope (Carl Zeiss, Oberkochen, Germany). Silique length was measured (5 siliques per line for 3 independent biological replicates) and siliques were dissected using a 27.5-gauge needle (Becton Dickinson, Franklin Lakes, NJ) to observe seed setting using a dissecting microscope (KEYENCE, Japan).

1-3. Results

1-3-1 Generation of the *A. thaliana* accession C24 mutant population

In order to develop a new reverse genetic resource, *A. thaliana* accession C24 seeds were treated with EMS. Optimum EMS concentrations of 20-45 and 20-50 mM have previously been reported for Col-0 and L*er* accessions respectively (McCallum et al. 2000, Martín et al. 2009). Nonetheless, because natural genetic variation (*e.g.*, reproductive system plasticity or DNA repair mechanisms) among accessions can greatly affect the optimum EMS dosage (Martín et al. 2009), we began by assessing the proper EMS concentration for *A. thaliana* accession C24 seeds. We determined suitable EMS concentrations based on two parameters: 1) the frequency of M_1 seed germination (Fig. 1-1A), and 2) the frequency of albino chimera M_1 seedlings (Fig. 1-1B). The frequency of M_1 seed germination was greatly reduced with incremental increases in EMS concentrations (Table 1-1). At EMS concentrations of ≥25 mM, the germination rate was less than 40% (Table 1-1). Meanwhile, the frequency of albino chimera seedlings increased as EMS concentrations rose (Table 1-1). A high percentage of albino chimera seedlings was observed from seeds treated with 30 mM (4.0%) and 40 mM EMS (7.2%; Table 1-1). Although higher EMS concentrations were predicted to induce higher mutation frequencies, this effect could be offset by reduced seed germination and viability (Martín et al. 2009). Thus, to generate the C24 mutant population, we elected to treat seeds with 25 mM EMS, which produced acceptable germination rates (37.0%) and albino chimeras (1.4%).

From approximately 8,000 seeds treated with 25 mM EMS, 3,620 M_1 seedlings were obtained, all of which were used to generate the M_2 population. An M_2 population with a total of 3,509 individual plants was successfully recovered for use in TILLING. This M_2 population also contained 77 partial seed set lines (semi-

sterile) and 125 very low seed set lines (sterile) (Table 1-2). This population of semi-sterile and sterile seed sets represents a potentially valuable resource for use in forward genetic screens to isolate novel genes affecting reproduction. Each M_2 plant sampled for DNA which was used in TILLING was originally isolated from an individual M_1 plant to ensure independence of mutations within the population. Finally, DNA from M_2 plants and M_3 seeds of 3,509 lines were stored for TILLING analysis. I designated this population of mutant lines the C24TILL collection.

1-3-2 Detection of EMS mutations from the C24TILL collection

To evaluate the quality of the C24TILL collection, five genes namely *DUO1* (At3g60460), *EXO70C2* (At5g13990), *EXO70H2* (At2g39380), *APK1b* (At2g28930), and *PKA* (At2g20050) were selected for TILLING analysis (Table 1-3). These selected genes either had no reported T-DNA lines available (*DUO1*, *EXO70C2*, *EXO70H2*) (Borg et al. 2011, Li et al. 2010) or were thought to be involved in the self-incompatibility (SI) signalling pathway (*APK1b*, *PKA*) (Murase et al. 2004, Kakita et al. 2007), which requires the C24 genetic background for functional analysis. Mutations in four selected genes namely *DUO1*, *APK1b*, *PKA*, and *EXO70C2* were evaluated from a functional standpoint. Detailed mutations found in the *EXO70H2* are listed in Supplemental Table 2. From a total of 11,805 bp fragments screened, 86 mutations were obtained (Table 1-3). These were verified by sequencing and comprised 63.9% missense, 25.6% sense, 1.2% nonsense (premature stop codon), and 9.3% intronic mutations. Of these, 31 mutations (~30%) were homozygous, fulfilling the expected 1:2 proportion for homozygous/ heterozygous M_2 plants. This result also suggests that detection of heterozygotes (relative to homozygotes) was not noticeably compromised by pooling (Greene et al. 2003). It has been reported that EMS predominantly induces G/C to A/T transitions, with

guanine residues being the primary target of alkylation producing O^6-ethylguanine, which pairs with T instead of C (Greene et al. 2003). This mechanism predicts a strong G/C to A/T bias in EMS-treated mutant populations, which has been observed in numerous mutagenesis studies (Greene et al. 2003). Accordingly, 97.6% of the mutations were G/C to A/T substitutions, with 73.8 % of changes at G and 26.2 % at C on the coding strand.

In order to estimate the average density of detected mutations per line, mutation density was calculated according to the following formula: (size of fragment screened) (number of plants screened) / (number of identified mutants). The average mutation density was calculated after subtracting 40 base pairs (derived from the common primers) from each gene. Based on the five candidate genes screened, the average mutation density in the C24TILL collection to be 1/433 kb (Table 1-3).

1-3-3 Functional characterization of *duo1* mutants

In order to demonstrate the utility of the C24TILL resource, TILLING mutants obtained in the *DUO POLLEN 1* (*DUO1*) gene were further characterized. DUO1 is a male germline-specific essential MYB transcription factor which has been identified in two separate genetic screens (Park et al. 1998; Rotman et al. 2003). Previously described truncation mutations in *DUO1*, *duo1-1* (C to T nonsense mutation at nucleotide 812) from the No-0 accession, and *duo1-2* (14 bp insertion at nucleotide 672) from the C24 accession, resulted in a single larger diploid sperm cell that is unable to fertilize egg cells (Rotman et al. 2005). Because *DUO1* is an essential gene for sperm cell specification, a homozygous mutant line cannot be obtained and further studies on *DUO1* function require partial loss of function mutants. In the TILLING analysis of the C24TILL collection, seven mutations within the 1,436 bp *DUO1* gene fragment were obtained (Fig. 1-3A). Of these, one was

nonsense, two were missense, and the rest were silent mutations (Fig. 1-3A). A mutation from G to A at nucleotide 159 created a premature stop codon in *DUO1*, and this line was tentatively named *duo1_159*. The other characterized lines included two missense mutations, *duo1_641* and *duo1_782*, in which Arg residues at positions 214 and 261 were substituted with Ile and Ser, respectively.

The only heterozygous line obtained was *duo1_159*, which had a shorter silique (average length, 7.8 mm; *cf.* 12.7 mm in wild type; Fig. 1-4B). In the siliques of *duo1_159*, about half of the ovules were not fertilized and were aborted (Fig. 1-4C). Consistent with the previous analysis of *duo1-1* and *duo1-2* (Rotman et al. 2005), this abortion phenotype was dependent on pollen-related defects. In heterozygous *duo1_159*, approximately half of the pollen grains had a single diploid sperm cell that was unable to fertilize (Fig. 1-4A). In contrast to *duo1_159*, two missense lines, *duo1_641* and *duo1_782*, produced homozygous lines with normal siliques that were indistinguishable from wild-type (WT) (Fig. 1-4B, C). The process of sperm cell specification also appeared normal in these missense lines, which produced tricellular pollen with two intensely staining sperm cell nuclei similar to WT (Fig. 1-4A). These observations suggest that these missense mutations lines did not affect DUO1 function as related to sperm cell specification.

1-4. Discussion

1-4-1 Establishment of C24TILL collection

I have established a new reverse genetic tool for *A. thaliana* accession C24 by generating an EMS mutagenized population, designated the C24TILL collection, for use in combination with the TILLING screening method. The development of the

C24TILL collection described here represents the third TILLING resource reported for *A. thaliana* to date (Table 1-4). To ensure an adequate amount of mutations are present in this collection, a suitable EMS concentration was determined and used. On average, the lines of this new C24TILL collection carry one mutation every 433 kb, which is slightly lower than the previously reported 1/300 kb in the Col-0 TILLING resource (Greene et al. 2003). However, it should be noted that, there are caveats in the C24TILL collection mutation density estimation, including the possibility that certain gene fragments were not effectively screened resulting in missed mutations. By contrast, the estimated 1/89 kb mutation density obtained in the L*er* collection (Martín et al. 2009) remains the highest mutation rate reported to date for *Arabidopsis* TILLING resources.

As described by Martín et al. (2009), the mutation density differences between the TILLING populations of *A. thaliana* might be due to natural genetic variation between accessions for their tolerance to chemically induced mutations. In addition, the estimation of mutation density detected by TILLING can also be affected by uneven mutation detection along the gene fragments (Greene et al. 2003). Higher GC content in the analyzed fragments (41%) than in the genome at large (35%) can also cause bias in TILLING mutation density estimation (Martín et al 2009; AGI 2000). Despite all these factors and caveats, I have successfully established a new C24TILL collection which can provide substantial interesting mutations for functional genomics studies in *A. thaliana* accession C24. The availability of the current C24TILL collection enables deeper functional genetic studies, especially for researchers aiming to understand novel gene functions in this unique C24 genetic background. The established C24TILL collection will also serve as a valuable complementary tool alongside existing reverse genetic tools to allow a better understanding of gene functions in *Arabidopsis*.

1-4-2 TILLING for *duo1* leaky mutant

TILLING the C24TILL collection for *DUO1* identified an allelic series of induced point mutations, including sense, missense and silent mutations. Further analysis of the *duo1_159* nonsense mutant demonstrated its genotype/phenotype correlation in male gametophyte development. Because homozygous *DUO1* mutation is lethal, I sought to screen for *duo1* leaky mutants using TILLING from the C24TILL collection. Previously, leaky mutants were successfully recovered for *COI1*, which encodes an F-box protein involved in jasmonate signalling (Xu et al. 2002), *ABA1*, which encodes a zeaxanthin epoxidase that functions in abscisic acid biosynthesis (Koornneef et al. 1982; Karssen et al. 1983), and *CESA3*, which is involved in cellulose synthesis (Ellis et al. 2002).

However, in this study the attempt to obtain a homozygous *duo1* leaky mutant with partial loss of function was unsuccessful. Characterization of the two homozygous missense mutation lines, namely *duo1_641* and *duo1_782* showed no aberrant pollen grain phenotype as compared to wild-type (Fig. 1-4). This is not unexpected as the point mutations in both lines did not significantly impact protein function as predicted by SIFT (sorting intolerant from tolerant). SIFT predicts whether an amino acid substitution will affect protein function that potentially alter the phenotypes (Ng and Henikoff 2003). SIFT scores less than 0.05 indicate that the amino acid substitution is likely to affect protein function (Ng and Henikoff 2003). Both missense lines showed SIFT scores of 1.00, indicating no predicted deleterious impact on protein function. Nevertheless, this study successfully demonstrated that an array of mutations could be identified for *DUO1* from the established C24TILL collection.

1-5. Figures and tables

A

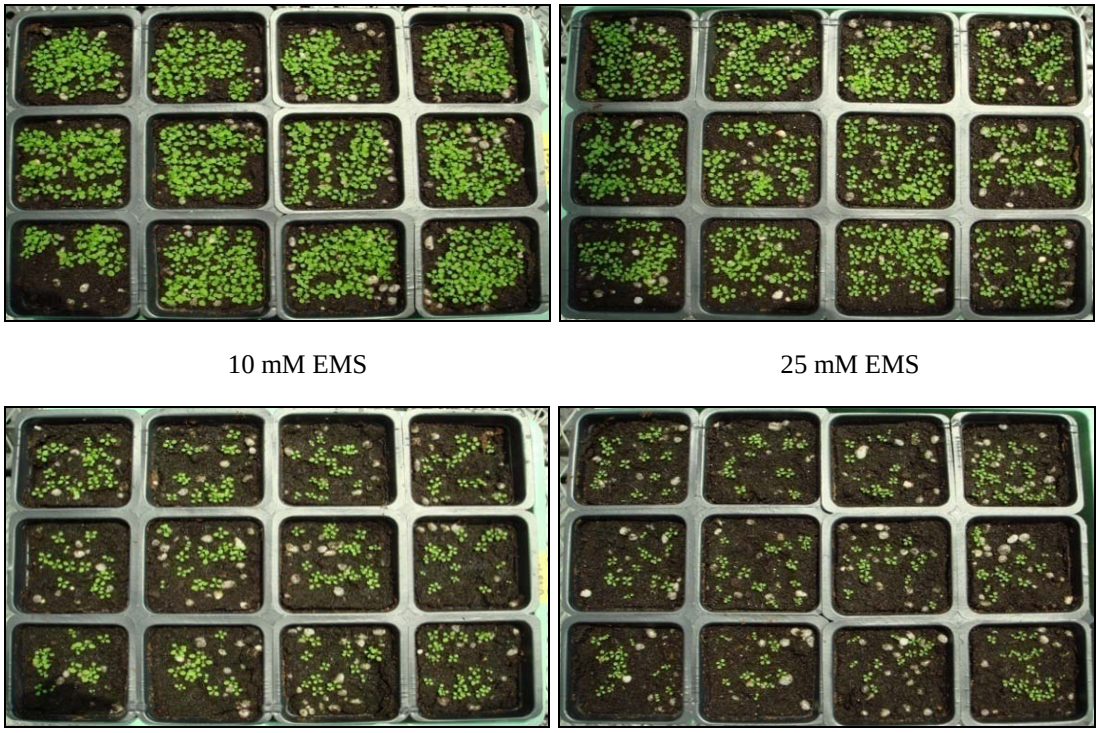

10 mM EMS 25 mM EMS

30 mM EMS 40 mM EMS

B

Figure 1-1. Generation of EMS mutagenized *A. thaliana* accession C24. (A) Dose effects of EMS mutagenesis on M_1 seeedlings (14 days after sowing). (B) Albino chimera phenotype observed in M_1 mutagenized plant.

Table 1-1. Dose effects of EMS mutagenesis in *A. thaliana* C24 M_1 plants

Phenotype	EMS concentration (mM)			
	10	25	30	40
Seed germination rate (%)*	84.0%	37.0%	35.5%	33.5%
Albino chimera seedling (%)*	0%	1.4%	4.0%	7.2%

*Data were recorded on 600 seed batches for each treatment.

Table 1-2. Summary of seed set phenotype observed in M_2 plants

	Total	Fertile	Semi sterile	Sterile
M_2 population (lines)	3509	3307	77	125

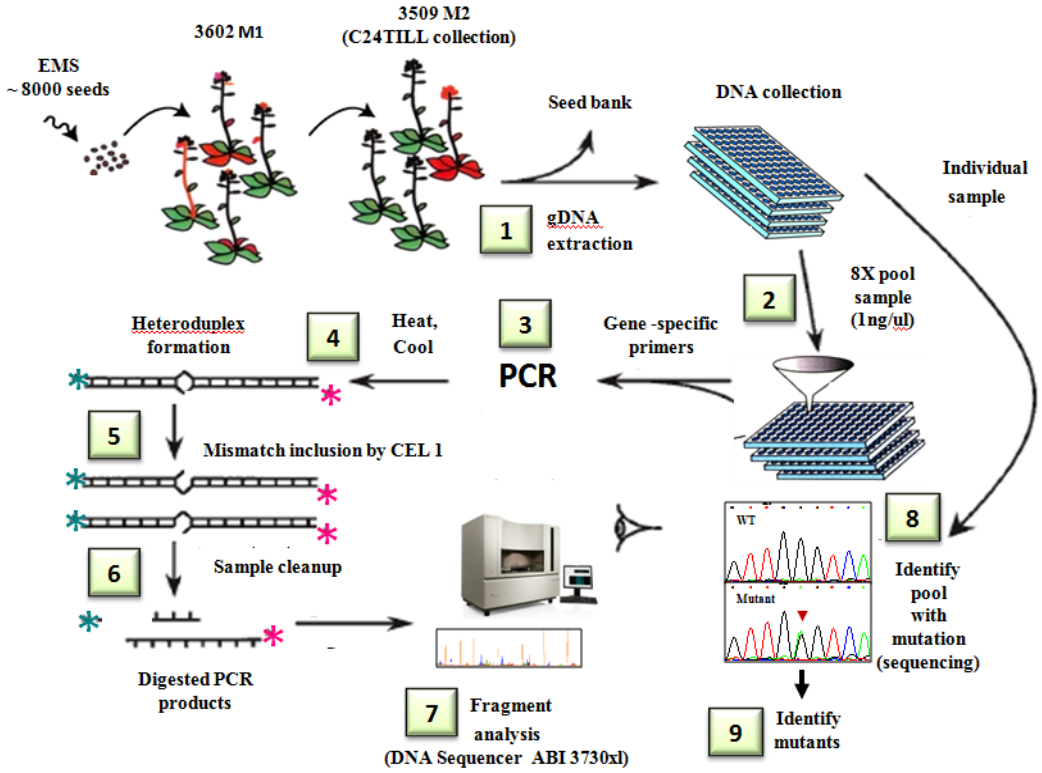

Figure 1-2. Outline of TILLING for C24TILL collection. (1) Genomic DNA (gDNA) extraction from M_2 mutants. (2) Equalization and pooling of DNA samples. (3) Amplification of target gene by PCR. (4) Denaturation and reannealing of PCR products. (5) Heteroduplex digestion with CEL 1 endonuclease. (6) Samples cleaning for removal of salts and buffer component. (7) Samples loading and detection of mutations using capillary DNA sequencer. (8) Individual mutation detection from DNA pool sample. (9) Target mutant lines identified from seed bank (diagram modified from Till et al. 2003).

Table 1-3. Mutations in 5 selected genes found by TILLING the C24TILL collection

Gene	Amplicon length (bp)	Number of screened lines	Total screened length (kb)	Number of obtained mutation					*Mutation density (kb^{-1})
				Total	Missense	Sense	Nonsense	Intronic	
DUO1 At3g60460	1436	3072	4289	7	2	4	1	0	1/613
EXO70C2 At5g13990	2076	3456	7036	29	22	7	0	0	1/243
EXO70H2 At2g39380	2127	3456	6651	28	21	7	0	0	1/258
APK1b At2g28930	2205	3072	7213	9	3	2	0	4	1/739
PKA At2g20050	3961	3072	12045	13	7	2	0	4	1/871
Total	11805	16128	37234	86	55	22	1	8	1/433

*Mutation density (kb^{-1}) was estimated after subtracting 40 bp of the length of universal primers for overall gene fragment screened.

Table 1-4. EMS mutagenized TILLING resources in the *Arabidopsis*

Species	Ploidy level	Population size (lines)	Mutation density per line (kb^{-1})	Reference
1. *A. thaliana* (Co1)	2x	3072	1/300 kb	Greene et al. 2003
2. *A. thaliana* (Ler)	2x	3712	1/89 kb	Martín et al. 2009
3. *A. thaliana* (C24)	2x	3509	1/433 kb	Lai et al. in press (present work)

A

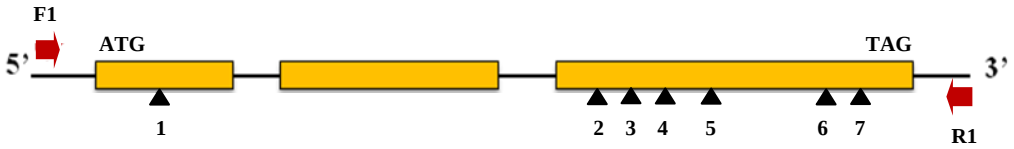

***DUO1* (At3g60460)**

No	Position from ATG	Exon/ Intron	Amino acid change	Homo/ Hetero	Mutation type
1	G 159 A (*duo1_159*)	Exon	W 53 X	Hetero	Nonsense
2	G 641 A (*duo1_641*)	Exon	R 214 S	Homo	Missense
3	C 678 T	Exon	-	Homo	Sense
4	C 687 T	Exon	-	Hetero	Sense
5	C 782 T (*duo1_782*)	Exon	R 261 I	Homo	Missense
6	G 966 A	Exon	-	Homo	Sense
7	G 972 A	Exon	-	Hetero	Sense

B

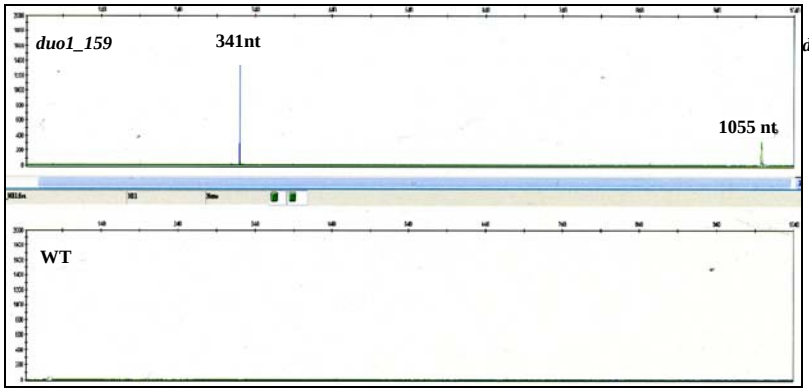

C

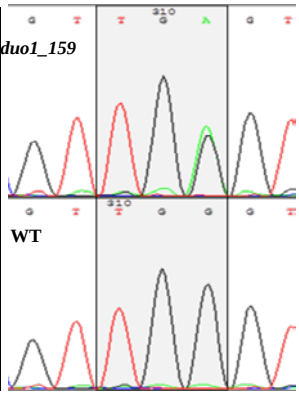

Figure 1-3. Seven point mutations were identified in the *DUO1* gene. (A) Detailed analysis of mutations found in the *DUO1* gene fragment. Diagram shows the analysed *DUO1* gene fragment and the locations of detected mutations (black arrowheads). The position of forward and reverse primers used for TILLING screen are indicated by red arrows. (B) Electropherograms of *DUO1* gene fragment of *duo1_159* and WT plants.(C) Sequencing chromatograms around mutation site of heterozygous *duo1_159* and WT plants. The original tryptophan codon (TG**G**) and the stop codon (TG**A**) created by G to A transition (at nucleotide 159) are shown in shaded boxes.

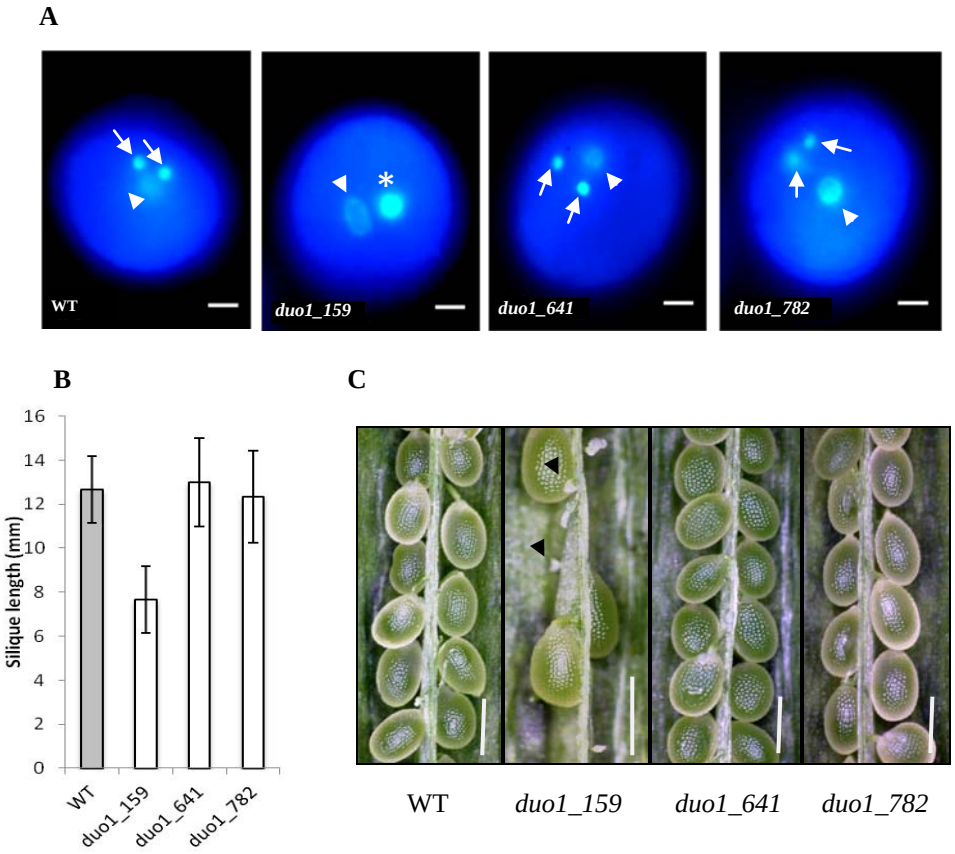

Figure 1-4. Functional characterization of *duo1* mutants. (A) DAPI staining of *duo1* mutant pollen. The DAPI-stained vegetative cell nuclei and sperm cell nuclei are indicated by arrowheads and arrows, respectively. A single larger generative cell nucleus is indicated by an asterisk. Bars: 10 μm. (B) Length of *duo1* mutant siliques. (C) Seed set analysis of *duo1* mutants. Aborted ovules are indicated by black arrowheads. Bars: 1 mm.

Chapter 2

Functional characterization of *APK1b* and *PKA* in self-incompatible signalling of *Arabidopsis thaliana* accession C24

2-1. Introduction

In the Brassicaceae (crucifer) family, the self-incompatibility (SI) reaction is based on allele-specific interactions between two highly polymorphic proteins encoded by the *S*-locus haplotype: *S*-locus receptor kinase (SRK), a single-pass transmembrane serine/threonine kinase displayed on the surface of stigma epidermal cells (Takasaki et al. 2000), and its ligand *S*-locus protein 11 (SP11 or SCR), a small secreted protein localized in the pollen coat (Schopfer et al. 1999; Takayama et al. 2000). Under one current model of SI signalling, contact between a pollen grain and stigma epidermal cell allows the binding of SP11 to the extracellular domain of its cognate SRK receptor to take place. Upon interaction, SRK undergoes autophosphorylation and, together with the plasma membrane-tethered MLPK (M-locus Protein Kinase) (Murase et al. 2004), phosphorylates Armadillo Repeat-Containing protein 1 (ARC1) (Stone et al. 1999), a U-box E3 ubiquitin ligase. Recently, EXO70A1, a putative component of the exocyst complex which functions in polarized secretion in yeast and animals was identified as an ARC1 interacting partner (Samuel et al. 2009). Overexpression of *EXO70A1* in stigma epidermal cells has been reported to cause partial breakdown of SI (Samuel et al. 2009). In both *Brassica* and *Arabidopsis*, reduction of *EXO70A1* expression levels disrupts compatible pollen tube growth (Samuel et al. 2009). Consistent with these results, EXO70A1 has been suggested to be involved in compatible pollination and to be targeted by ARC1 for ubiquitination and degradation, thereby precluding the

secretion of compatibility factors that support compatible pollen hydration, germination and tube growth (Samuel et al. 2009).

A hallmark of SI study in Brassicaceae is the generation of *A. thaliana* exhibiting SI as a result of transformation with *SRK* and *SP11* derived from its self-incompatible sister species, *Arabidopsis lyrata* (Nasrallah et al. 2002). Some *A. thaliana* accessions, such as Columbia (Col-0), RLD, and WS-0 exhibit transient SI when introduced with *SRK* and *SP11* (i.e., stigma only express SI response during a narrow developmental window, but subsequently lose their ability to reject self pollen) while C24 accession expresses a developmentally stable SI response indistinguishable from that exhibited by naturally SI *A. lyrata* plants (Nasrallah et al. 2004). This finding implies that some *A. thaliana* accessions have retained all required downstream components of SI signalling. The availability of these self-incompatible *A. thaliana* (SI *A. thaliana*) provides new opportunities for exploiting the tools of this tractable model plant to dissect the SI response in Brassicaceae. Indeed, this SI model plant has begun to fulfil its promise specifically when a hypomorphic allele of *PUB8* gene that caused transient SI (Liu et al. 2007) and when RNA-dependent RNA polymerase RDR6, which functions in trans-acting siRNA production thereby acting as negative regulator of SI (Tantikanjana et al. 2009), were identified from studies using this model plant. Besides, the *Arabidopsis* orthologs of known *Brassica* SI components, *AtAPK1b* (*BrMLPK*), *AtPUB17* (*BrARC1*) and *AtEXO70A1* (*BrEXO70A1*) were also identified. However, the SI role of these orthologs in *Arabidopsis* SI signalling remain controversial.

In our laboratory, previous studies have identified cAMP-dependent protein kinase A (PKA) as a potential MLPK interactor by yeast two-hybrid screening (Kanatani 2008). PKA in the *Brassica* pistil cDNA library was shown to interact with the active form of MLPK kinase domain (Kanatani 2008). However, the biological function of PKA in SI signalling pathway remains unknown.

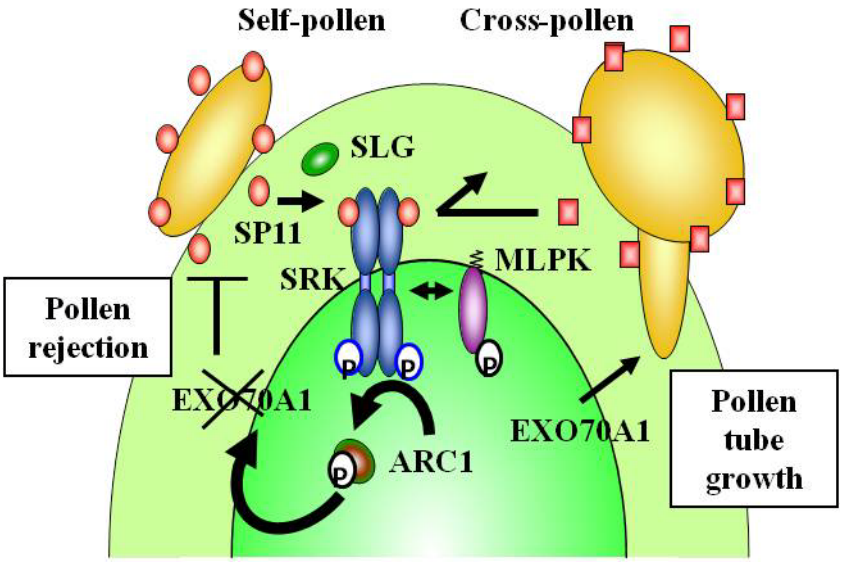

Figure 2-1. Model for SI signalling pathway in the Brassicaceae. Following the landing of self pollen on the stigmatic papillae, SP11 ligand will bind to its SRK receptor and activates the SI signalling. SRK will then undergo autophosphorylation and together with MLPK interact with, and phosphorylates ARC1. This in turn stimulates ARC1-mediated proteasomal degradation of EXO70A1, thus leading to the rejection of self-incompatible pollen.

Having established the C24TILL collection, I aimed to screen for *apk1b* and *pka* mutants using TILLING method. Along with the TILLING mutants, I also performed stigma specific RNAi-based silencing to down regulate the expression of *APK1b* and *PKA*. In addition, an *apk1b* mutant including non-functional kinase domain was also generated and overexpressed. Using these mutant lines, I tested the involvement of *APK1b* and *PKA* in SI signalling of transgenic *Arabidopsis*. The results do not support a functional role of these genes in SI *A. thaliana*. I further discuss the implications of these results on our understanding of the SI signalling pathway.

2-2. Materials and methods

2-2-1 Plasmid constructs

To make RNAi constructs for *APK1b* and *PKA*, 350 bp *APK1b* and *PKA* fragments were amplified by PCR and cloned into the pENTR-TOPO vector (Invitrogen, USA). Using LR clonase (Invitrogen, USA), *APK1b* and *PKA* fragments were subcloned in inverse orientation into the pANDA vectors (Miki and Shimamoto 2004) under the control of the stigma-specific *AtS1* promoter. The construct to overexpress (under the control of *AtS1* promoter) non-functional *APK1b* (*APK1b*^{K117R}), harbouring the mutation at nucleotide 353 (A to G) was kindly provided by Dr. Mitsuru Kakita. These constructs were introduced into *Agrobacterium tumefaciens* strain GV3101 (pMP909) and transform into C24 accession plants using the floral dip method as described previously (Clough and Bent 1998). Gene-specific primers are listed in Supplemental Table 1.

2-2-2 Plant materials and TILLING mutants

RNAi and overexpression transgenic plants were prepared by transforming the constructs into *A. thaliana* C24 plants homozygous for the *SRK* transgene using the floral dip method as described previously (Clough and Bent 1998). The *apk1b* and *pka* TILLING mutants were obtained by TILLING the C24TILL collection. These mutants were crossed to the transgenic C24 plants homozygous for the *SRK* transgene. F_1 progenies from this cross were selfed to obtain F_2 progenies containing *SRK and APK1b* or *SRK and .PKA* transgenes.

2-2-3 Quantitative real-time PCR

Total RNA was extracted from stigmas using the RNeasy Plant Mini Kit (Qiagen, USA) and treated with DNase I (Invitrogen, USA). The concentration and purity of total RNA was determined by spectrophotometric analysis. First-strand cDNA was synthesized from 1 μg of total RNA using SuperScript II reverse transcriptase (Invitrogen, USA). Quantitative real-time PCR was performed using the One-step QuantiTect SYBR Green RT-PCR kit according to the manufacture's protocol (Qiagen, USA). Data were collected using the Roche Light Cycler 480 sequence detection system according to the manufacturer's instructions (Roche, Germany). Gene-specific primers are listed in Supplemental Table 1.

2-2-4 Characterization of *apk1b* and *pka* mutant phenotypes

Pollination assays were performed by hand-pollinating pre-emasculated stigmas with pollen. Aniline blue staining was performed in pollinated pistils collected 8 h after pollination and stained as described by Sumie et al. (2001). Stained pistils were

observed and photographed with a Zeiss Axioplan fluorescence microscope (Carl Zeiss, Oberkochen, Germany). Pollen hydration was evaluated after 30 min of pollination on the papilla cells.

3-3. Results

2-3-1 Analysis of *apk1b* mutant phenotype

The *A. thaliana APK1b* gene belongs to the Receptor-like Cytoplasmic Kinase VII (RLCK VII) subfamily of protein kinases. Of all members of this subfamily in *Arabidopsis*, *APK1b* is the closest ortholog based on the highest sequence similarity (76% at the amino acid identity), genomic synteny and genomic structure to *Brassica MLPK* (Kakita et al. 2007). In order to test the involvement of *APK1b* in SI, the C24TILL collection was screened for *apk1b* mutants. A total of nine *apk1b* TILLING mutants were identified (Fig. 2-2A). From these mutants, three missense mutation lines (Fig. 2-2A) were crossed to the transformed C24 plants homozygous for the *SRK* transgene. F_1 progenies derived from this cross were selfed to obtain F_2 progenies homozygous for the *APK1b* missense mutation and with *SRK* transgene, and used for SI functional analysis. Pollen hydration assays showed that all of these *apk1b* homozygous missense mutants exhibited SI phenotype (Fig. 2-2C). Further pollination assays also suggested that introgression of these missense mutations into the *SRK*-expressing C24 line did not change the self-incompatible phenotype (i.e. rejection of *SP11*-expressing pollen) (Fig. 2-2B).

To complement the TILLING mutants, I also generated *APK1b*-suppression lines using RNAi construct driven by the stigma specific *AtS1* promoter in C24 plants homozygous for *SRK* transgene. Of several transformants analyzed, two transgenic

plants with the strongest reduction of stigma *APK1b* transcripts were selected for analysis (Fig. 2-3A). Consistent with the observations in *apk1b* TILLING mutants, pollination assays using these *APK1b* RNAi lines showed no significant changes in SI phenotype (Fig. 2-3B). These RNAi lines expressed SI phenotype indistinguishable from the positive control plants.

To further test the involvement of *APK1b* in SI, I next tried to generate a dominant-negative line by overexpressing the kinase-dead *APK1b* (*APK1b*^{K117R}) in C24 plants homozygous for *SRK* transgene. Previously, *APK1b*^{K117R} mutation in the conserved Vla kinase subdomain has been shown to result in abolished kinase activity (Kakita et al. 2007). Sequencing of PCR products amplified from *APK1b*^{K117R} overexpressing plant cDNA was performed to detect the level of *APK1b*^{K117R} expression (Fig. 2-4A). Several transformants exhibiting a ~2 to 3 fold increase in stigma *APK1b*^{K117R} expression relative to wild-type were tested for SI phenotype (Fig. 2-4A). Pollination and pollen hydration assays, did not indicate pollen tube penetration into the stigmas (Fig. 2-4B) nor pollen hydration (Fig. 2-4C) in *APK1b*^{K117R} overexpressing plants.

Consistent with the observations of *APK1b* mutants in this study, Kitashiba et al. (2011) reported similar results. Using a T-DNA line (Col-0 background) with no detectable *APK1b* transcripts crossed to Col-0 plant homozygous for *SRK* and *SP11* transgenes, they observed no weakening of SI phenotype from the pollination assay. Moreover, results of RNAi suppression of *APK1b* transcripts (C24 background) are also consistent with and complement the *APK1b* RNAi data obtained in this study.

2-3-2 Analysis of *pka* mutant phenotype

PKA belongs to the Protein Phosphatase 2C (PP2C) family of genes (Xue et al. 2008). Members of the PP_2C family from various organisms have been implicated as negative

modulators of protein kinase pathways activated by diverse developmental signalling cascades (Xue et al. 2008). Previous works in our laboratory have identified PKA as a potential interactor to MLPK (Kanatani 2008). In this study, seven *pka* missense mutants were identified from the C24TILL collection using TILLING (Fig. 2-5A). After introgressing these missense mutations into C24 plants homozygous for *SRK* transgene, I tested the involvement of *PKA* in SI. The seven missense mutation lines tested showed no apparent SI phenotype changes in pollination (Fig. 2-5B) and pollen hydration (Fig. 2-5C) assays.

In addition, I also generated *PKA* RNAi lines in C24 plants with *SRK* transgene to further test the function of *PKA* in SI. Two transformants with the strongest reduction of stigma *PKA* transcripts were used for SI phenotype analysis (Fig. 2-6A). Supporting the analysis of *pka* TILLING mutants, RNAi transformants also exhibited no observable SI phenotype changes in pollination assay (Fig. 2-6B). Again, this result implies that, PKA does not play functional role in *Arabidopsis* SI.

2-4. Discussion

Molecular genetic studies of SI in non-model self-incompatible species, in particular *Brassica*, can be difficult to perform. The lack of genomic tools and relatively laborious transformation methods for *Brassica* make SI studies difficult. The establishment of self-incompatible *A. thaliana* transgenic system (Nasrallah et al. 2002) has enabled us to exploit the genomic tools of this model plant for understanding SI. However, stable and robust SI could be obtained in very limited *A. thaliana* accessions, such as C24. In contrast, a large reservoir of genomic resource for this tractable model plant has been developed in different and limited accessions, such as Col-0 and L*er*. Therefore, the

C24TILL collection established in this study will make a great contribution especially for the studies of SI.

Generally, signalling pathways that underlie the same biological processes should be conserved over long evolutionary time spans (>100 million years) (Antunes et al. 2009, Lam et al. 2011), and this conservation is used to justify the use of *Arabidopsis* as a model system to understand biological processes in related non-model plants. Since the evolutionary divergence of *Brassica* and *Arabidopsis* is estimated to be ~14 to 20 million years, SI signalling cascade is unlikely to have undergone drastic modification (Koch et al. 2001, Yang et al. 1999). Therefore, our early hypothesis that the functional analysis of *APK1b* (ortholog of *Brassica MLPK*) and *PKA* would reveal these proteins to be functional in *Arabidopsis* SI is plausible. Unfortunately, several lines of evidence from this study were negative against our expectation for both *APK1b* and *PKA* genes.

Assuming that the discrepancy depends on the difference in plant materials, following explanation can be possible. First, the SI signalling components underlying the two taxa (*Arabidopsis* and *Brassica*) may be different. Although this scenario seems unlikely based on conservation, one should not rule out the possibility that the evolutionary divergence between *Arabidopsis* and *Brassica* might have altered the downstream actors in the SI pathway between these taxa. Second, *APK1b* belongs to the RLCK VII subfamily, which is comprised of 46 members (Shiu et al. 2003), some of which are closely related to *APK1b*. RLCK VII kinases are expected to be somewhat redundant (Kakita et al. 2007). Therefore, other RLCK VII kinases may have masked or assumed the functional role of *APK1b* in SI.

Because null mutant for *APK1b* and *PKA* could not be obtained in this TILLING search, I could not definitely judge the involvement of these genes in *Arabidopsis* SI. The missense mutations of *APK1b* and *PKA* mutants tested in this study may not have deleterious impact on the protein function. In addition, incomplete suppression of

APK1b and *PKA* transcripts in RNAi lines used in this study may also be inadequate to weaken the SI phenotype. Hence, analysis using mutants with completely abolished *APK1b* and *PKA* transcripts should be needed to further reconcile the role of these genes in *Arabidopsis* SI.

2-5. Figures

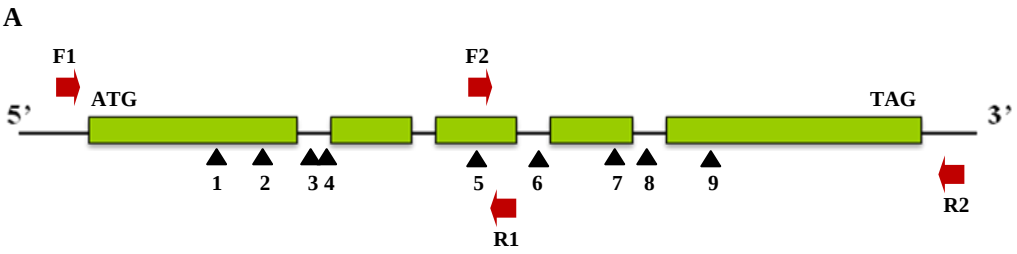

***APK1b* (At2g28930)**

No	Position from ATG	Exon/ Intron	Amino acid change	Homo/ Hetero	Mutation type
1	G 474 A (*apk1b_474*)	Exon	C 23 Y	Hetero	Missense
2	G 606 A (*apk1b_606*)	Exon	S 67 N	Homo	Missense
3	G 841 A	Intron	-	Homo	Intronic
4	G 848 A	Intron	-	Hetero	Intronic
5	G 1155 A	Exon	-	Hetero	Sense
6	G 1302 A	Intron	-	Hetero	Intronic
7	G 1366 A	Exon	-	Hetero	Sense
8	G 1498 A	Intron	-	Hetero	Intronic
9	A 1804 C (*apk1b_1804*)	Exon	N 354 S	Homo	Missense

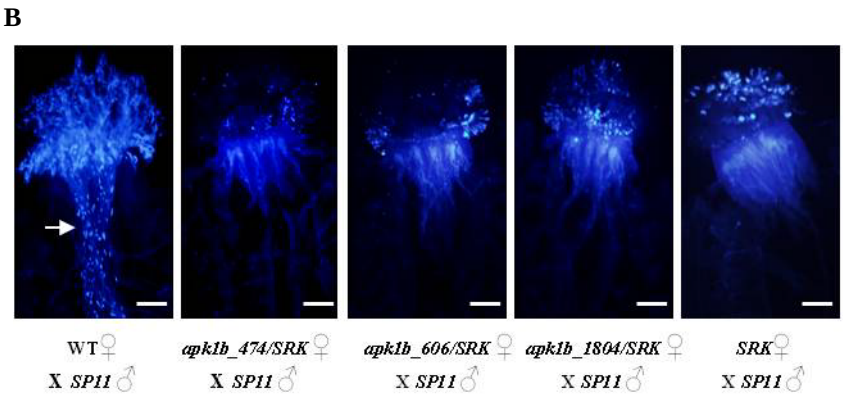

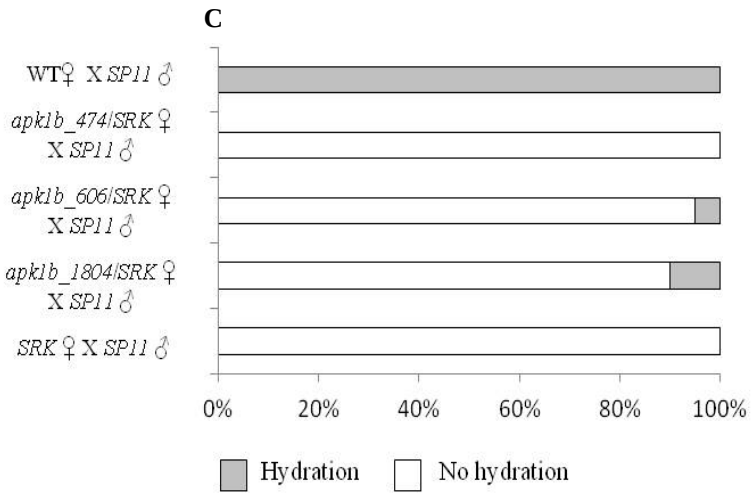

Figure 2-2. Characterization of *apk1b* TILLING mutants. (A) Detailed analysis of mutations found in the *APK1b* gene fragment**.** Diagram shows the analysed *APK1b* gene fragment and the location of detected mutations (black arrowheads). Forward and reverse primer sites for TILLING analysis are indicated by red arrows. (B) Pollination assays of *apk1b* TILLING mutants. Aniline blue was used as a fluorescent dye to visualize pollen tubes penetration. Pollen tubes are indicated by white arrow. Bars: 200 μm. (C) Pollen hydration assays of *apk1b* TILLING mutants, n= 20 pollen.

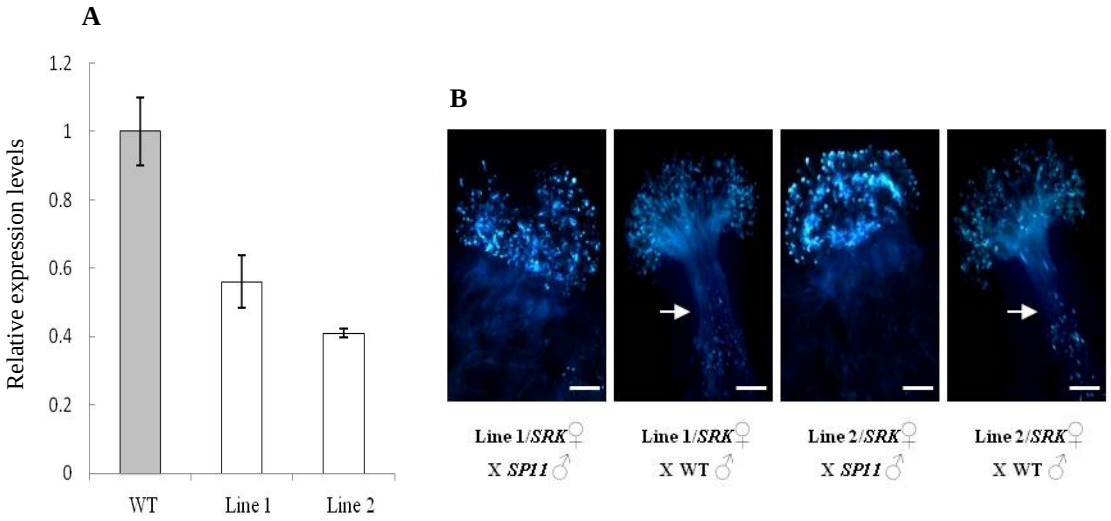

Figure 2-3. Expression and functional analysis of *APK1b* suppressed plants. (A) Quantitative real-time PCR analysis of *APK1b* transcripts in the stigmas of WT plant and *APK1b* RNAi transformants (lines 1 and 2). (B) Pollination assays of *APK1b* RNAi plants. The stigmas of WT and *APK1b* RNAi C24 plants homozygous for *SRK* transgene were pollinated with *SP11*-expressing pollen. Aniline blue was used as a fluorescent dye to visualize pollen tube penetration. Pollen tubes are indicated by white arrows. Bars: 200 μm.

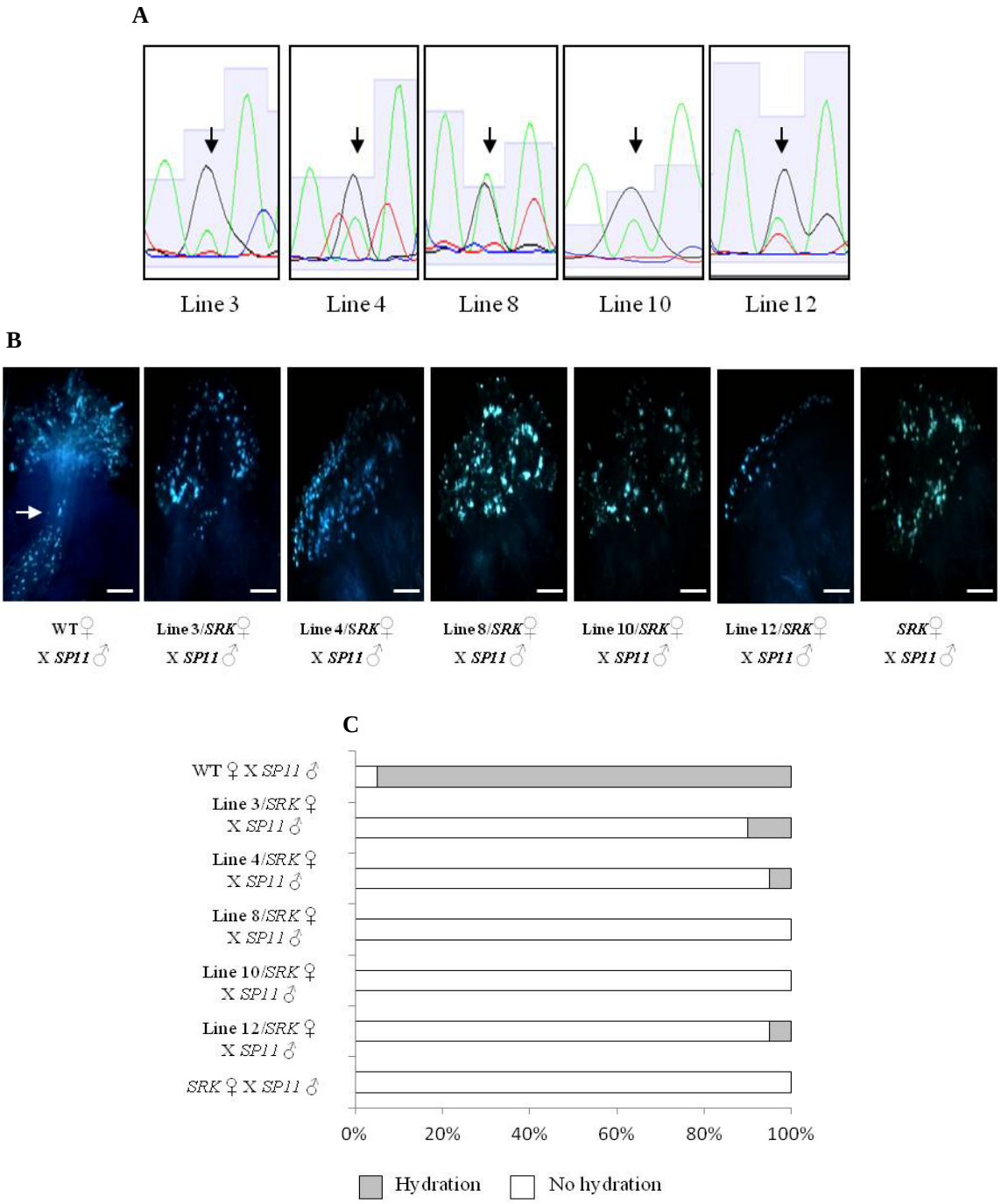

Figure 2-4. Expression and functional analyses of *APK1b*^{K117R} overexpressing plants. (A) Comparative expression analyses of endogenous *APK1b* (green peak) and *APK1b*^{K117R} transgene (black peak) in *APK1b*^{K117R} overexpressed lines. Electropherograms around the mutated nucleotide (A**A**A->A**G**A, Lys->Arg) which is indicated by black arrows. (B) Pollination assays of *APK1b*^{K11R} overexpressing C24 stigmas with *SRK* transgene using *SP11*-expressing pollen. Aniline blue was used as a fluorescent dye to visualize pollen tubes penetration. Pollen tubes are indicated by white arrow. Bars: 200 µm. (C) Pollen hydration assays of *APK1b*^{K11R} overexpressing plants, n= 20 pollen.

A

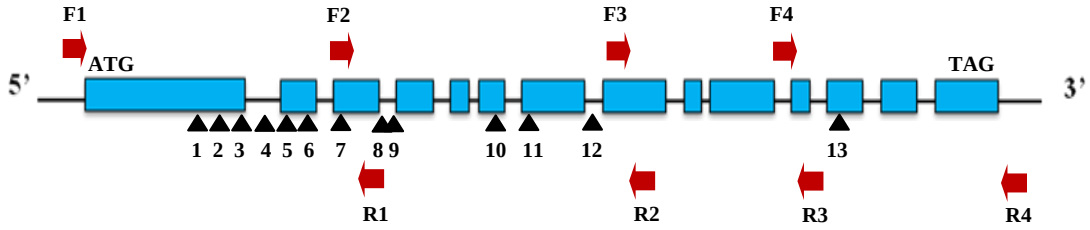

***PKA* (At2g20050)**

No	Position from ATG	Exon/ Intron	Amino acid change	Homo/ Hetero	Mutation type
1	A 679 G (*pka_679*)	Exon	R 227 G	Hetero	Missense
2	T 748 C (*pka_748*)	Exon	F 250 L	Homo	Missense
3	T 773 C (*pka_773*)	Exon	V 258 A	Homo	Missense
4	G 1094 A	Intron	-	Hetero	Intronic
5	G 1218 A	Exon	-	Homo	Sense
6	G 1245 A	Exon	-	Hetero	Sense
7	G 1446 A (*pka_1446*)	Exon	E 424 K	Hetero	Missense
8	G 1620 A	Intron	-	Hetero	Intronic
9	G 1655 A	Intron	-	Hetero	Intronic
10	A 2097 G (*pka_2097*)	Exon	R 550 G	Homo	Missense
11	A 2258 T (*pka_2258*)	Exon	N 572 Y	Hetero	Missense
12	G 2534 A	Intron	-	Hetero	Intronic
13	G 3722 A (*pka_3722*)	Exon	R 925 K	Hetero	Missense

B

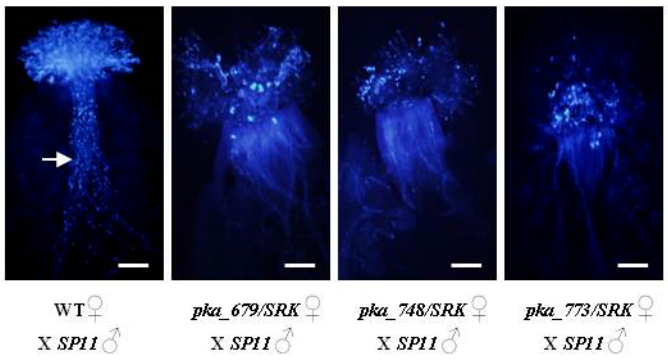

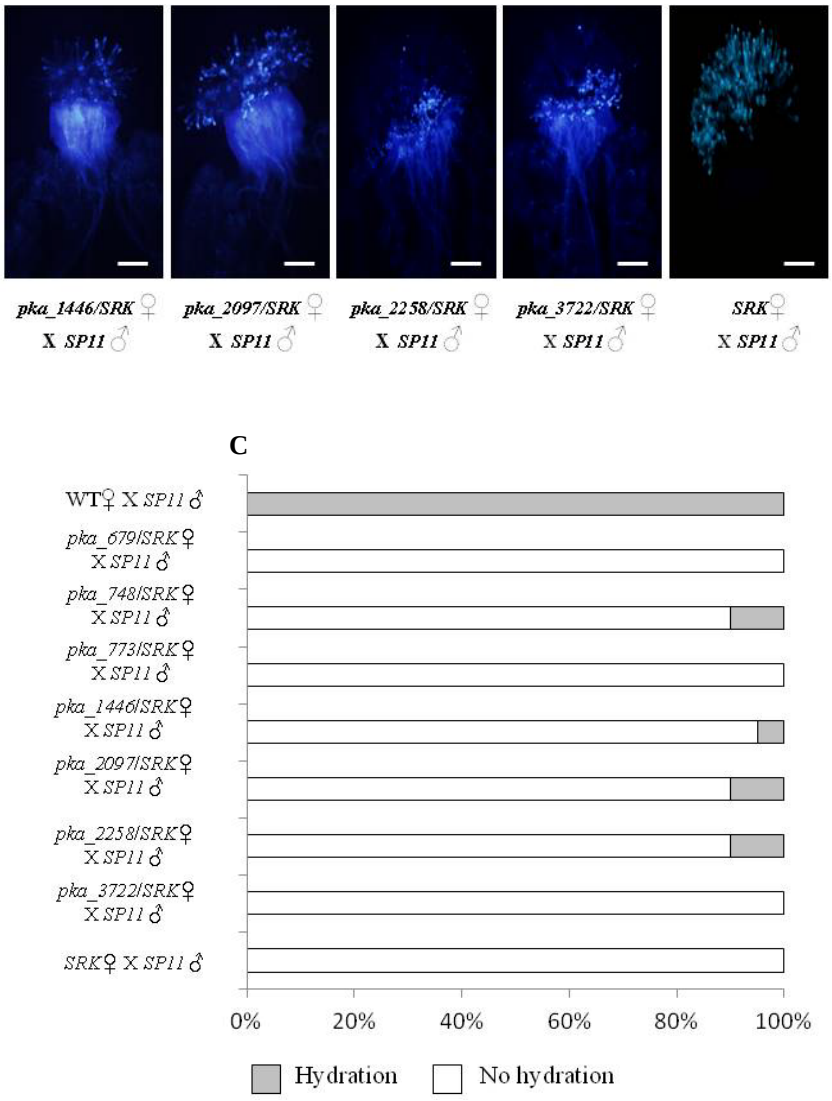

Figure 2-5. Characterization of *pka* TILLING mutants. (A) Detailed analysis of mutations found in the *PKA* gene fragment**.** Diagram shows the analysed *PKA* gene fragment and the location of detected mutations (black arrowheads). Forward and reverse primer sites for TILLING analysis are also indicated by red arrows. (B) Pollination assays of *pka* missense mutants. Each missense mutant was introgressed into C24 lines with *SRK* transgene, and pollinated with *SP11*-expressing pollen to check the SI phenotype. Aniline blue was used as a fluorescent dye to visualize pollen tubes penetration. Pollen tubes are indicated by white arrow. Bars: 200 μm. (C) Pollen hydration assays of *pka missense* mutants, n= 20 pollen.

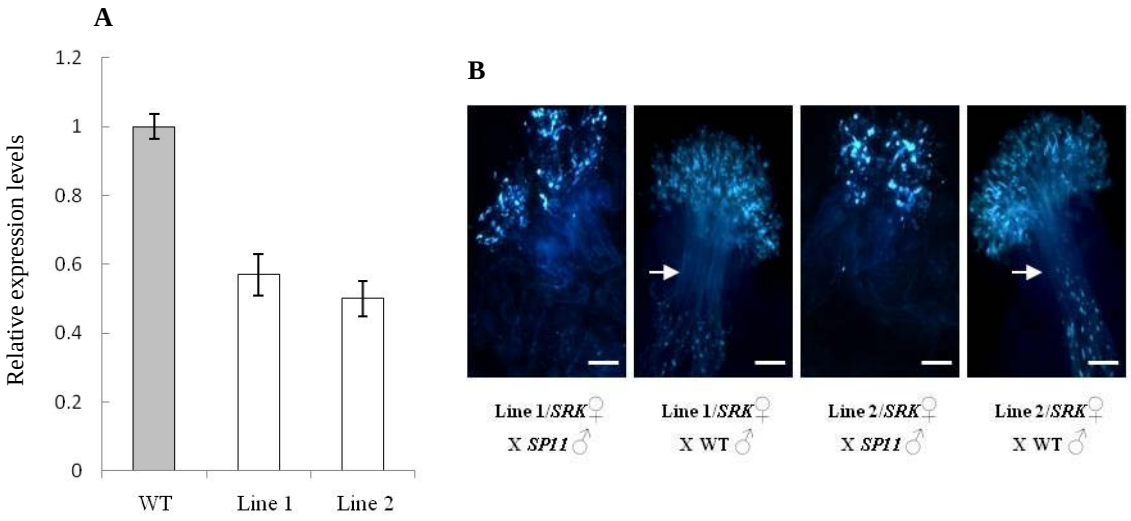

Figure 2-6. Expression and functional analysis of *PKA* suppressed plants. (A) Quantitative real-time PCR analysis of *PKA* transcripts in the stigmas of WT plant and *PKA* RNAi transformants (lines 1 and 2). (B) Pollination assays of *PKA* RNAi transformants. Each *PKA* RNAi transformants with *SRK* transgene was pollinated with WT and *SP11*-expressing pollen. Aniline blue was used as a fluorescent dye to visualize pollen tubes penetration. Pollen tubes are indicated by white arrows. Bars: 200 μm.

Chapter 3

Functional characterization of *EXO70C2* in pollen development

3-1. Introduction

Vesicle traffic either through the plasma membrane or via the eukaryotic endomembrane system is facilitated by various tethering factors (Sztul and Lupashin 2006). These molecules act as molecular bridges that provide initial interactions between vesicles and their target membranes, thus ensuring proper targeted secretion (Hala et al. 2008). Examples of these tethering factors are GARP (Golgi-associated retrograde protein), Dsl1 complexes, COG (conserved oligomeric Golgi), and exocyst (an octameric protein complex) (Songer and Munson 2009).

To date, exocyst is the only proposed tethering factor required for regulation of various exocytosis processes in plants (Zhang et al. 2010). Exocyst is an octameric protein complex which mediates the tethering of post-Golgi secretory vesicles to the plasma membrane for exocytosis (Munson and Novick 2006). It is comprised of eight subunits, SEC3, SEC5, SEC6, SEC8, SEC10, SEC15, EXO70, and EXO84 (Hsu et al. 2004, Tsuboi et al. 2005). In *Arabidopsis*, SEC6 and SEC8 are each encoded by a single gene, SEC3, SEC5, SEC10, and SEC15 are each encoded by two genes, EXO84 is encoded by three genes and EXO70 by 23 genes (Zhang et al. 2010). Mutation of maize *SEC3* homolog *RTH1* results in small stature and short root hairs (Wen et al. 2005). Moreover, SEC3 was demonstrated to interact with ROP GTPases via an ICR adaptor protein in *Arabidopsis* (Lavy et al. 2007). Mutants in other exocyst subunits such as *SEC5*, *SEC6*, *SEC8*, *SEC15*, and *EXO70A1* exhibit defects in root hairs and pollen tube growth (Cole et al. 2005; Wen et al. 2005; Synek et al. 2006; Hala et al. 2008; Zarsky et

al. 2009). Meanwhile, EXO84b was shown to participate in cytokinesis and cell plate maturation in *Arabidopsis* (Fendrych et al. 2010). All these studies imply that the exocyst complex plays an important role in regulating development and polarized cell growth in plants.

The large and specific expansion of the EXO70 family may represent a mechanism of regulation for plant exocysts to specify their function for various exocytosis (Zhang et al. 2010). T-DNA insertion in *EXO70A1* causes the disruptions of polarized cell growth and plant development (Synek et al. 2006). EXO70A1 was also proposed to participate in pollen-stigma interaction by exporting cellular materials essential for pollen hydration (Samuel et al. 2009). In addition, EXO70B2 and EXO70H2 were shown to be involved in plant defence, and were proposed to deliver essential components for formations of cell wall appositions during pathogen attacks (Pecenkova et al. 2011). Finally, mutation of *EXO70C1* leads to retardation of pollen tube growth (Li et al. 2010).

Recent expression analyses show that five *EXO70* genes namely *EXO70C1*, *EXO70C2*, *EXO70G2*, *EXO70H3*, and *EXO70H5*, are expressed in the stamen and pollen (Synek et al. 2006; Wang et al. 2008; Chong et al., 2010; Li et al. 2010). These genes are expressed in overlapping but different patterns, suggesting roles in different vesicle trafficking processes during pollen development and pollen tube growth (Li et al. 2010). During pollen tube growth, the establishment of a narrow growth site at the plasma membrane of growing tip requiring continuous targeting of Golgi-derived vesicles to this site and their fusion with the plasma membrane is essential for proper polarized cell growth (Miller et al. 1997; Yang 1998; Cole and Fowler 2006; Emons and Ketelaar 2009; Zarsky et al. 2009).

Highly active vesicle trafficking processes also occur in microspores and tapetal cells during pollen development (Scott et al. 2004). The exocyst has been proposed to

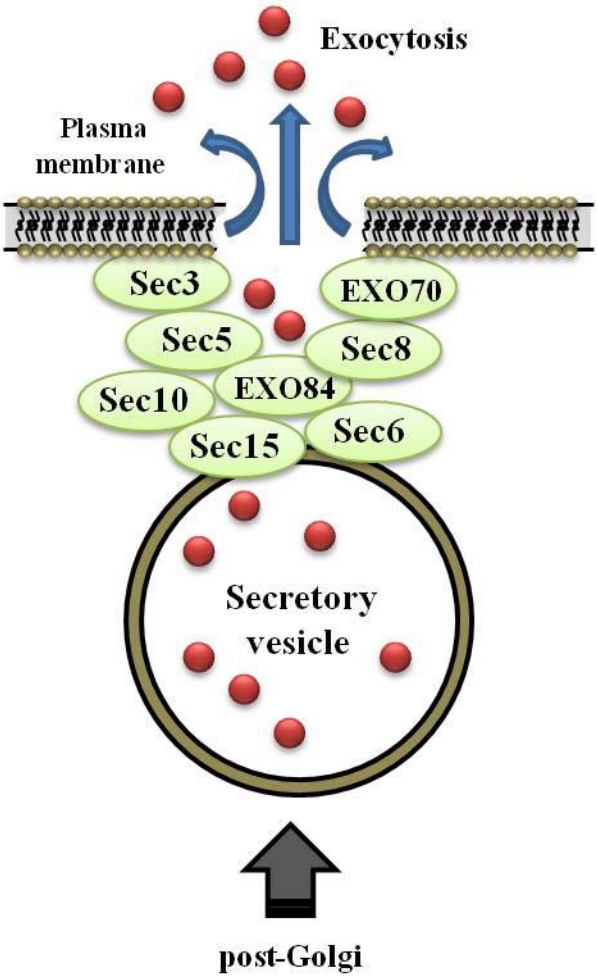

Figure 3-1. A model for function of the exocyst complex in tethering the secretory vesicles to the plasma membrane in plants. The exocyst subunits (Sec3, Sec5, Sec6, Sec8, Sec10, Sec15, EXO70, and EXO84) are represented by green circles. The exocyst complex binds the secretory vesicle derived from Golgi body and tether the vesicle to the plasma membrane for exocytosis.

function in targeted secretion during pollen cytokinesis (Otegui and Staehelin 2004). Exocyst-like structures connecting vesicles during cell plate formation in *Arabidopsis* cells were observed by electron tomography (Otegui and Staehelin 2004; Segui-Simarro et al. 2004; Otegui et al. 2005). In addition, during the tapetum degradation process, various vesicles containing precursors or nutrients are properly targeted and fuse with the plasma membrane to release their contents into the anther locule to support pollen development (Wilson and Zhang 2009). Previously, *Male gametgenesis Impaired Anthers* (*MIA*) gene was proposed to be required for proper secretion of vesicle cargo to the plasma membrane during pollen development (Jakobsen et al. 2005). T-DNA insertional mutants of *MIA* produce aborted pollen grains and exhibit a severe reduction in fertility (Jakobsen et al. 2005). Moreover, a mutation in *MS1*, the Plant Homeodomain (PHD) transcription factor that regulates pollen wall material secretion causes failure to produce viable pollen (Vizcay-Barrena and Wilson 2006).

Based on the importance of proper targeted vesicle secretion and cell type-specific expression during pollen development, I anticipated that mutations in *EXO70* genes might lead to defect in the cell types where the genes are expressed, as long as there is no redundancy. Here, I provide experimental data demonstrating that EXO70C2, a subunit of the exocyst complex is required for pollen development in *Arabidopsis*. Because T-DNA mutants with reduced or abolished *EXO70C2* expression cannot be obtained, I performed TILLING to screen for *exo70c2* mutants in the C24TILL collection. The *exo70c2* mutants exhibit defects in pollen development and seed sets. Mutant pollen grains are aborted with abnormal morphology. In addition, I show that *EXO70C2* is localized to the cytoplasm and preferentially expressed in pollen. Using *in situ* hybridization, I further confirm that *EXO70C2* is expressed in pollen and tapetum during pollen development. My data illustrate the importance of EXO70C2 in pollen development.

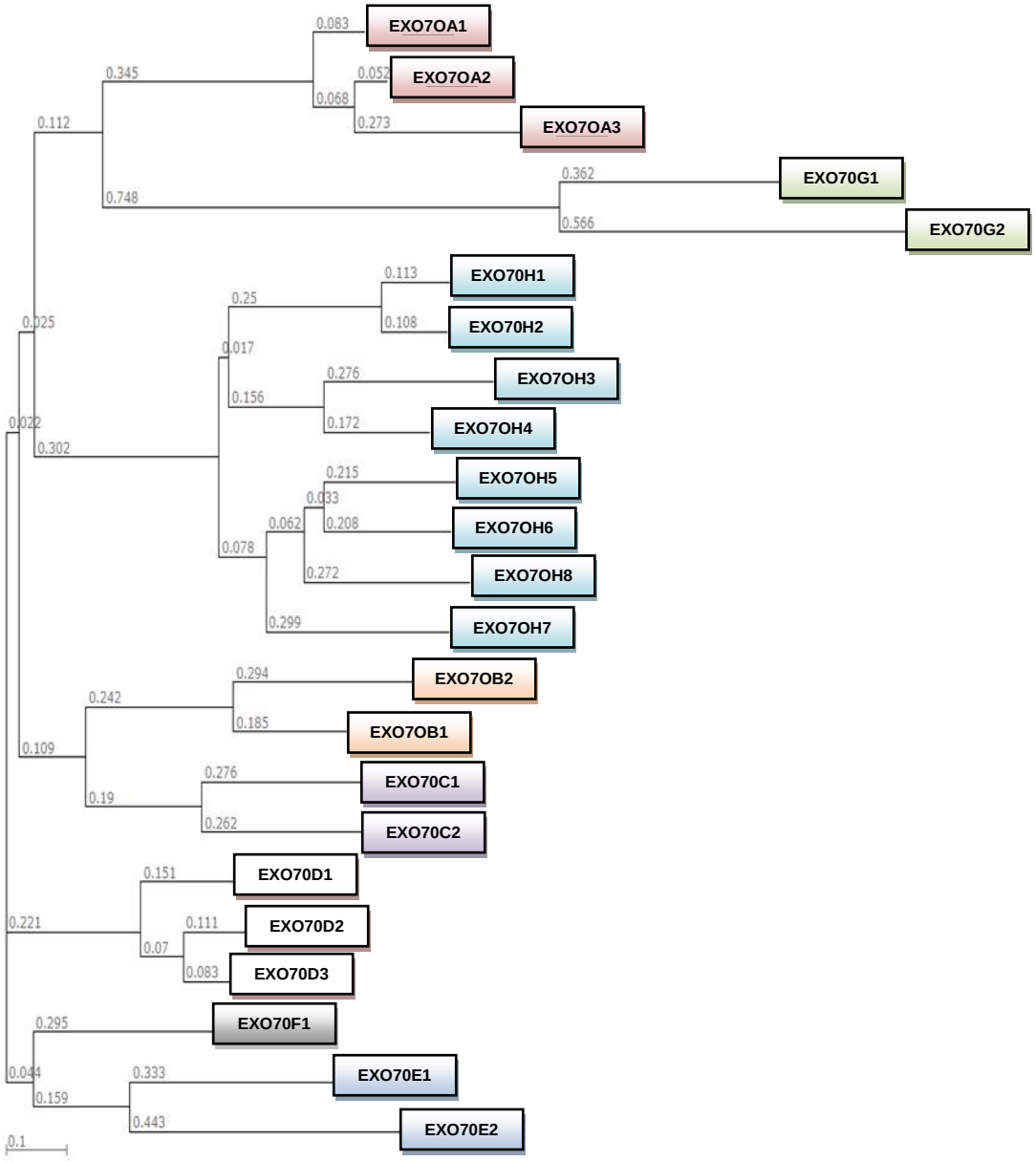

Figure 3-2. Phylogenetic analysis of the plant EXO70 family. The tree was constructed by aligning protein sequences using MAFFT version 6 (http://mafft.cbrc.jp/alignment/server/). Eight EXO70 clusters are highlighted with shading.

3-2. Materials and methods

3-2-1 Plant materials and TILLING mutants

The *A. thaliana* (Col-0) *EXO70C2* T-DNA line (SALK_045767) was obtained from Nottingham Arabidopsis Stock Centre (http://arabidopsis.info/). Homozygous insertion in *EXO70C2* was validated in the F_2 population by PCR. To test the presence of the full-length gene product, total RNA extraction and cDNA synthesis were performed as described in Chapter 2-2-3. RT-PCR was performed using gene-specific primers and *ACTIN8* was used as a control. *exo70c2* mutants were obtained by applying TILLING in the C24TILL collection as described in Chapter 1-2-3. Mutations were verified by sequencing. Gene-specific primers are listed in Supplemental Table 1.

3-2-2 Characterization of *exo70c2* mutant phenotype

Plants were photographed with a Nikon D700 digital camera (Nikon, Japan). Flowers, siliques, and seeds were photographed using a dissecting microscope (KEYENCE, Japan). To analyze pollen germination in vitro, mature pollen grains were collected and cultured on medium containing 0.01% (w/v) H_3BO_3, 1mM $CaCl_2$, 1 mM $Ca(NO_3)_2$, 1 mM MgSO4, and 18% sucrose solidified with 0.5% (w/v) agar (pH 7.0). Pollen grains were cultured for 12 h, in 22℃ with 80% relative humidity and cool light. Germinated pollen grains were observed under a Zeiss Axiovert 135 microscope (Carl Zeiss, Oberkochen, Germany) and images were captured using AxioVision 4.7 software. Pollination assays were performed on pre-emasculated stigmas as described in Chapter 2-2-4. DAPI staining and aniline blue staining was performed as described in Chapter

1-2-4 and Chapter 2-2-4 respectively. Alexander staining was performed on mature pollen grains to detect pollen viability according to Alexander et al. (1969). Stained pollen grains were observed under a Zeiss Axiovert 135 microscope (Carl Zeiss, Oberkochen, Germany) and images were taken using AxioVision 4.7 software. Silique length measurement and seed setting observations were performed as described in Chapter 1-2-4. Seed counts were performed on siliques of six week old plants. Sterilized seeds were planted on vertical agar plates containing 1/2 strength MS medium (Sigma, USA) and root length of 14 days old seedlings was measured.

3-2-3 Quantitative real-time PCR and GUS assay

Quantitative real-time PCR was performed on total RNA extracted from various tissues and anthers of different development stages according to the protocol described in Chapter 2-2-3. The *ACTIN8* was used as a control. The *EXO70C2* promoter (1,136 bp upstream from ATG) was amplified and fused into pENTR/D-TOPO (Invitrogen, USA). The fragment was then recombined into pBGGUS destination vector using Gateway technology (Invitrogen, USA). The construct was introduced into *Agrobacterium tumefecians* strain GV3101 (pMP90) and transformed into wild-type *A. thaliana* C24 using the floral dip method as described previously (Clough and Bent 1998). Seven independent T_3 plants lines were subjected to GUS staining according to the protocol described by Jefferson et al. (1987). Samples were cleared as described by Malamy and Benfeny (1997). GUS staining images were taken using an Olympus BX51 microscope (Olympus, USA). Gene-specific primers are listed in Supplemental Table 1.

3-2-4 Subcellular localization of EXO70C2

The 35S:CFP:EXO70C2, 35S:YFP:PEP3, and 35S:tdTomato:H3 constructs were made by PCR cloning the corresponding full-length cDNAs into pENTR/D-TOPO (Invitrogen, USA). Using LR Clonase (Invitrogen, USA), the fragments were recombined into the pH35G destination vector series according to the manufacturer's instructions. The 35S:CFP was used as a control. *Arabidopsis* mesophyll protoplasts were isolated and prepared according to the method described by Yoo et al. (2007). 15 μg of each construct was transformed into isolated protoplasts using the PEG method as described previously (Yoo et al. 2007). LSM 510 META Confocal microscopy (Carl Zeiss, Germany) was used to examine protoplasts at 12 h after transformation with incubation at 25°C.

3-2-5 Light microscopy and cryo-scanning electron microscopy

Flower buds with anthers of different development stages were collected based on the size of bud and fixed with 2.5% glutaraldehyde in 0.05 M phosphate buffer, pH 7.2 for 2 h at 4°C. Samples were rinsed with 0.05 M phosphate buffer and postfixed in 1% OsO4. Following sequential ethanol dehydration, samples were embedded in Spur epoxy resin (Polysciences, USA). Transverse sections of 1 – 2 μm were cut using a Leica Ultracut UCT ultramicrotome (Leica, Wetzlar, Germany) and stained with 0.25% toluidine blue O and observed using a Zeiss Axiovert 135 microscope (Carl Zeiss, Oberkochen, Germany). Mature flowers and anthers were mounted onto cryo-SEM

stubs and plunged into liquid nitrogen. The frozen samples were viewed with a FEI QUANTA^{TM} 50 series SEM (FEI, USA).

3-2-6 *In situ* hybridization

The flower buds with anthers of different development stages were collected from wild-type *A. thaliana* C24. Digoxigenin-labeled and non-labeled *EXO70C2* antisense oligo probes were purchased from Nihon Gene Research Laboratory. The cDNA antisense sequences used was 5'-AGAAAGGCGACGTCGTTTCGGATGCTCATCCCTCAG ATGATGCGCATCATCAGGATGGTA-3'. *In situ* hybridization to 14 μm thick Paraplast (Sigma-Aldrich, USA) sections of formaldehyde-fixed flower buds was performed as described previously (Kakita et al. 2007). Briefly, excised flower buds were fixed in freshly prepared 4% paraformaldehyde for 1 h at 4°C. After washing with 0.05 M phosphate buffer, pH 7.2 for five times at 10 min interval, the sample was incubated overnight at 4°C. Samples were then dehydrated in a series of ethanol washes before embedding in paraffin (Sigma, USA) and sectioned (14 μm) for probing as described by Langdale (1994). Treated sections were hybridized with probe solution (10 mg/ml salmon sperm, 10 mM Tris, pH 8.0, probes, 5 mM EDTA, pH 8.0, 0.3 M NaC1, 10% dextran sulphate, 40% formamide, and 1X Denhart's solution) at 45°C overnight. After hybridization, sections were washed with 2X SSC for 1 h at 45°C, RNase treated (10 mg/ml RNase, 0.5 M NaCl, and 10 mM Tris, pH 8.0) at 37°C for 20 min and washed again with 2X SSC (twice for 30 min) at 45°C, with a final wash in 1X SSC for 15 min at room temperature (RT). Detection of hybrids was performed using anti-digoxigenin antibody (1:500, Roche, Germany), incubated overnight at RT before

washing with TBS solution (3 times) for 5 min at RT. Signal detection was performed using Fast^{TM} BCIP/NBT (Sigma, USA) and images were photographed using a Zeiss Axioplan fluorescence microscope (Carl Zeiss, Oberkochen, Germany).

3-3. Results

3-3-1 TILLING for *exo70c2* mutants

To address the function of EXO70C2 in *Arabidopsis*, I attempted to acquire *EXO70C2* T-DNA insertion line from the T-DNA Express database (http://signal.salk.edu/cgi-bin/tdnaexpress). No T-DNA insertion within the *EXO70C2* coding region was identified in the search. Only, a line with a T-DNA insertion ~1.0 kb upstream of the *EXO70C2* ATG start codon (SALK_045767) was identified, which was used in this study (Fig. 3-3A). Unfortunately, this homozygous T-DNA line showed neither reduction nor disruption of *EXO70C2* expression (Fig. 3-3B). Further phenotypic analysis also showed no significant difference when compared to wild-type (Fig. 3-3C-J). Because a suitable T-DNA line could not be obtained, a TILLING screen for *exo70c2* mutants in the established C24TILL collection was performed. A total of 29 point mutations corresponding to 28 mutants (one mutant with two point mutations) were isolated from the TILLING screen (Fig. 3-4A). Based on the amino acid changes, 14 TILLING mutants with mutations likely to affect EXO70C2 functions were selected for phenotypic analysis (Fig. 3-4A).

3-3-2 Defects in pollen germination, pollen tube growth and reduce seed set in *exo70c2* mutants

Phenotypic analysis of 14 homozygous *exo70c2* TILLING mutants successfully identified three mutants with reduced silique length compared to wild-type plant (Fig. 3-4B). These mutants, namely *exo70c2_544/1631*, *exo70c2_1445*, and *exo70c2_1481* with mutations in a conserved EXO70 family C-terminal domain that result in the amino acid substitutions G182R/G544E, S482L, and S494N respectively, showed identical silique length defects with differening severity (Fig. 3-4C). The EXO70 C-terminal domain acts as a binding domain and functions to anchor the exocyst complex to the plasma membrane for targeted secretion (He et al. 2007). Previously, *exo70* mutant lacking the functional C-terminal domain results in secretion defects (He et al. 2007). Since *exo70c2_1445* exhibited the shortest silique length, this mutant line was used in subsequent studies. To rule out the possibility that unrecognized or background mutations might be responsible for the observed phenotype, homozygous *exo70c2_1445* mutant (*exo70c2_1445/ exo70c2_1445*) was backcrossed to wild-type at least three times before measurements were performed. Upon backcrossing and in line with earlier observation, the siliques of both heterozygous (*+/exo70c2_1445*) and homozygous (*exo70c2_1445/ exo70c2_1445*) mutants were reduced in size (Fig. 3-5A, B) and contained significant fewer seeds than wild-type plants (Fig. 3-5D). Heterozygous showed approximately 45% reduction in seed set, while homozygotes were almost completely sterile (Fig. 3-5E). However, the seed set of heterozygote could be restored to wild-type levels after hand pollination with its own anther, which was not the case in homozygote (Fig. 3-5F). Closer inspection also revealed the reduction or absence of growing pollen tubes within the pistil of *exo70c2* mutants (Fig. 3-5C). To determine the nature of sterility, reciprocal crosses between wild-type plants and *exo70c2* mutants were performed. Pollination of *exo70c2* mutant pistils with wild-type pollen resulted in normal seed set, whereas pollination of wild-type pistils with *exo70c2* homozygous

mutant pollen did not result in seed sets (Fig. 3-5G). This result indicates that the function of the female organs is not compromised in mutant flowers. Additionally, no obvious root (Fig. 3-12) or other vegetative growth defects were observed in *exo70c2* homozygous mutant.

Detailed analysis further revealed that *exo70c2* mutant pollen grains were distinctively smaller compared to wild-type pollen grains (Fig. 3-6B). Pollen of *exo70c2* mutant was unable to germinate and grow pollen tubes *in vitro* (Fig. 3-6D). The mature pollen grains viability of heterozygote was further examined using Alexander's staining procedure (Alexander 1969). Approximately half of the pollen grains were dark green, indicating the non-viability of mutant pollen (Fig. 3-6F). Defective mutant pollen nuclear division was next tested using DAPI staining. Pollen of *exo70c2* mutants was abnormal with no visible sperm cells, whereas wild-type pollen contains two intensely stained sperm cells (Fig. 3-6G, H). Taken together, these results demonstrate that the almost complete sterility of *exo70c2* homozygous mutants may be caused by abnormal development of pollen grains.

3-3-3 Transcription of *EXO70C2* and subcellular localization of EXO70C2

The expression pattern of *EXO70C2* in *Arabidopsis* was determined by qRT-PCR. *EXO70C2* was abundantly expressed in anther tissue but not in other tissues (Fig. 3-7A). Low expression of *EXO70C2* was also detected in mature root tissue (Fig. 3-7A). To further examine the cellular expression pattern of *EXO70C2* in *Arabidopsis*, a fusion construct carrying 5' promoter sequences fused to the *GUS* gene (EXO70C2pro:GUS) was generated. Seven homozygous T_3 transgenic lines harbouring this fusion construct were used for GUS staining. Consistent with qRT-PCR analysis, strong GUS staining signals were detected in the anther (Fig. 3-7D), pollen grains (Fig. 3-7E), and growing pollen tubes (Fig. 3-7K, L). Closer inspection also revealed a GUS signal in mature root

(Fig. 3-7M) and root hairs (Fig. 3-7N). The expression pattern of *EXO70C2* observed in this experiment is slightly different from what has been reported previously for *EXO70C2* promoter GUS assays (Li et al. 2010). Beside the strong GUS signal detected in male reproductive cells, GUS signal was not observed in the root of seven days old seedlings as reported by Li et al. (2010). Since the promoter length in both studies was approximately similar (~1.1 kb), this is not likely the source of discrepancy. Perhaps, the spatial and temporal expression of *EXO70C2* can only be significantly detected in mature root by qRT-PCR experiment (Fig. 3-7A). Nevertheless, these results demonstrate that *EXO70C2* is preferentially expressed in anther and pollen.

To characterize this exocyst complex protein in more detail, subcellular localization pattern of EXO70C2 in *Arabidopsis* protoplasts was analyzed. N-terminal CFP-tagged, cDNA of *EXO70C2* (35S:CFP:EXO70C2) was co-expressed with YFP-tagged cytoplasm marker (35S:YFP:PEP3) or tdTomato-tagged nuclear marker (35S:tdTomato:H3). In order to avoid potential mislocalizations as a result of protein overexpression, only cells displaying weak fluorescence were assessed. Overall, CFP-tagged EXO70C2 was distributed throughout the cytosol (Fig. 3-8F). This protein also co-localized with the YFP-tagged cytoplasm maker (Fig. 3-8G) but not the tdTomato-tagged nuclear marker (Fig. 3-8L). These results indicate that EXO70C2 is localized in the cytosol in *Arabidopsis*.

3-3-4 EXO70C2 is essential for pollen development

To observe the pollen morphology of *exo70c2* mutants in detail, pollen grains were examined using cryo-scanning electron microscopy (cryo-SEM). Anthers and pollen grains from wild-type plants appeared normal (Fig. 3-9G, J), whereas a number of collapsed and abnormal pollen grains were observed in the anthers from *exo70c2* mutants (Fig. 3-9H, K). The percentage of aborted pollen grains was consistent with

light microscopy (Fig. 3-6B) and seed set (Fig. 3-5B) observations. Pollen grains from *exo70c2_1445* homozygotes were almost completely collapsed and aborted (Fig. 3-9I, L).

To gain more insight into the expression pattern of *EXO70C2* during pollen development, anther development was divided into 14 stages (Fig. 3-10A) as described previously (Sanders et al. 1999). *EXO70C2* expression pattern was examined in detail during pollen development using promoter GUS assay, qRT-PCR analysis and RNA *in situ* hybridization. GUS signals were visible from postmeiotic pollen (stages 9 and 10) to mature pollen (stage 11) and pollen release stages (stages 13 and 14) (Fig. 3-10B). There was no detectable expression of *EXO70C2* during early pollen development and meiosis stages (stages 1 to 8) (Fig. 3-10B). In agreement with the promoter GUS assay data, *EXO70C2* transcript profiling using qRT-PCR also showed expression of *EXO70C2* at stages 9 to 14 (Fig. 3-10C). To more precisely determine the *EXO70C2* expression pattern during pollen development, I performed RNA *in situ* hybridization on wild-type floral sections. *In situ* hybridization was performed using anthers from stages 8 to 12 where high *EXO70C2* expression was detected. Strong *in situ EXO70C2* signals were detected in post meiotic pollen (stages 9 and 10), pollen mitotic division (stage 11), and pollen release stages (stages 13 and 14). Additionally, *EXO70C2* signal was also detected in tapetum (stages 9 and 10). Taken together, these results indicate that *EXO70C2* is specifically expressed in pollen and tapetum during pollen development.

Based on the *EXO70C2* expression pattern, transverse section of *exo70c2* mutant anthers from stages 8 to 14 were examined (Fig. 3-11). There was no detectable difference between wild-type and *exo70c2_1445* homozygotes at stages 8 and 9 (Fig. 3-11). Normal microspores, tapetum and pollen grains were found in both wild-type plant and *exo70c2_1445* homozygotes. Subsequently and supporting high *EXO70C2*

expression, abnormal pollen morphology was detected from stages 10 to 14 in mutant homozygotes (Fig. 3-11). Pollen grains from these stages were completely degenerated and collapsed. By contrast, mutant heterozygotes only exhibited partial pollen degeneration (Fig. 3-11). Collectively, these observations suggest that the *EXO70C2* mutation resulted in the defects in pollen development, further affecting male sterility in *Arabidopsis*.

3-4. Discussion

The eight subunits (Sec3, Sec5, Sec6, Sec8, Sec10, Sec15, EXO70, and EXO84) that form the exocyst complex have been extensively studied in both yeast and mammals (Guo et al. 1999, Mattern et al. 2001). The exocyst is involved in spatially regulated exocytosis by functioning in tethering secretory vesicles to plasma membranes prior to exocytosis. Unlike a single gene in yeast and most animal genomes, the *EXO70* family in plants has expanded greatly for unknown reasons (Synek et al. 2006, Chong et al. 2010, Zhang et al. 2010). Two hypotheses have been proposed by Synek et al. (2006) for the pronounced multiplication of *EXO70* genes in plants: (1) only some EXO70 proteins serve as subunits for plant exocyst complex, while others perform functions independent of exocyst; and (2) plants may be endowed with a number of different exocyst forms, each with a specific EXO70 subunit, which function differently. Recent studies suggest that the second hypothesis is most likely to be true. First, the expression of EXO70 members is associated with exocytosis-active cells and these genes are expressed specifically in one or several cell types (Li et al. 2010). Second, several *EXO70* members are expressed in pollen, roots and tip-growing cells but with defined temporal patterns suggesting that they may function independently but synergistically (Synek et al. 2006, Li et al. 2010). In line with these observations, mutations in several

EXO70 members lead to tissue-specific defects, further demonstrating that different EXO70 members function in a cell type- or cargo-specific manner with no overlapping function (Fendrych et al. 2010, Li et al. 2010, Pecenkova et al. 2011).

To further address the function of *EXO70* genes, I characterized *exo70c2* mutants and demonstrated that EXO70C2 is required for pollen development. In agreement with its strong pollen-restricted expression pattern (Fig. 3-7), mutation in *EXO70C2* resulted in aborted pollen grains and reduced fertility. Interestingly, similar observations were also reported for *exo70a1* mutants (Synek et al. 2006). The fact that both *EXO70C2* and *EXO70A1* are essential for pollen development indicates that these exocyst subunits are not functionally redundant. In addition to pollen development defects, *exo70a1* mutants also show a diverse range of vegetative growth defects (Synek et al. 2006), which are not observed in *exo70c2* mutants. Perhaps, as discussed above, they may both be required for pollen development but function independently in regulating different exocytosis processes. Previously, phylogenetic analysis showed that *EXO70C1* and *EXO70C2* share 45.7% amino acid similarity and belongs to a two-member subclade (Synek et al. 2006). Since only pollen tube growth defects were reported for *exo70c1* mutants (Li et al. 2010) and to rule out the possibility of genetic redundancy, we intended to examine the pollen morphology of *exo70c1* mutants. However, attempts to obtain the reported *exo70c1* mutant are unsuccessful because the reported line was discontinued. Nonetheless, several lines of evidence suggest that *EXO70C1* and *EXO70C2* have no overlapping function. Unlike *exo70c2* mutants with aborted pollen grains, *exo70c1* mutant pollen grains are able to germinate but with slower pollen tube growth (Li et al. 2010). This implies that, the pollen development in *exo70c1* mutant is normal. Collectively, previous studies along with current studies strongly support the notion that different EXO70 members regulate different vesicles for different exocytosis processes.

The aborted pollen grains observed in *exo70c2* mutants suggest that proper secretory processes are interfered with during pollen development. Since EXO70C2 is a subunits of the exocyst complex, it may play a role in regulating the proper tethering of vesicles crucial in pollen development. Based on the *EXO70C2* expression detected in pollen and tapetal cells, several possible scenarios can be proposed to explain the aborted pollen grains observed in this study. First, EXO70C2 may participate in cytokinesis during pollen development. In eukaryotes, cytokinesis depends on the proper targeting of exocytic vesicles *e.g.* either to the cell plate in plants or to the cleavage furrow in animals (Guertin et al. 2002), and the direct role in this process has been demonstrated in mammalian cells (Fielding et al. 2005; Gromley et al. 2005) and *S. cerevisiae* (Dobbelaere and Barral 2004; VerPlank and Li 2005). Upon completion of pollen meiosis (stage 7), active cytokinesis occurs to establish the primary cell wall between the microspores (stages 8 and 9). During cytokinesis, various arabinogalactan proteins, callose and cellulose synthase complexes are transported and deposited to the cell plate sites for the formation of a new cell wall (Crowell et al. 2009; Gutierrez et al. 2009). Previously, exocyst-like particles were observed by electron tomography to tether vesicles during the formation of the cell plate in developing *Arabidopsis* pollen (Otegui and Staehelin 2004). Hence, exocyst can act in trafficking of vesicles containing essential cell wall components and regulate the proper targeted secretion to generate new plasma membranes during cytokinesis in pollen. This is consistent with the role of exocyst in pectin delivery during seed coat development in *Arabidopsis* (Kulich et al. 2010). To further support this hypothesis, recently, Fendrych et al. (2010) reported the involvement of EXO84b, SEC6, SEC8, SEC15b, and EXO70A1 in cytokinesis and cell plate maturation of root meristem cells. In this study, strong *EXO70C2* expression was detected during the cytokinesis phase (stage 9) of pollen development (Fig. 3-10D), indicating its role in targeted secretion. The strong *EXO70C2* expression detected in stage 9 but not stage 8 (Fig. 3-10D) may further suggest its role in the final stage of

cytokinesis, where active trafficking of vesicles containing cell wall components occur to support cell wall maturation. Therefore, I hypothesize that cytokinesis in pollen is dependent on EXO70C2, and that the loss of function of this crucial exocyst subunit may affect cell wall establishment and lead to the abnormal pollen morphology observed in this study.

Second, *EXO70C2* expression detected in tapetum may also imply a role in tapetal cells to support pollen development. Successful pollen development, and thus reproduction, requires precise coordination and high secretory activity in both anther tissue and pollen (Jakobsen et al. 2005). The tapetal cells of *Arabidopsis* are of secretory type (Murgia et al. 1991) and supply array of proteins, lipids, precursors, and other nutrients required for pollen maturation (Zheng et al. 2003). The discharge of nutrients from the tapetum strictly depends on the precise and proper functioning of targeted secretion to support pollen maturation. Thus, the exocyst complex is expected to play a role in regulating active secretion processes in tapetal cells. In this study, *EXO70C2* expression was also detected in tapetum at stages 9 and 10 (Fig. 3-10D), where highly active secretion takes place. At these stages, right after microspores are released from the tetrad (stages 8 and 9) and before mitosis (stage 11), tapetum breakdown is initiated. During this degradation process, vesicles containing various essential components fuse with the plasma membrane to release their contents into the anther locule to support pollen maturation (Wilson and Zhang 2009). In agreement with the timing of tapetum degeneration, the pollen development defect was first detected at stage 10, when tapetum degeneration occurs, in *exo70c2* mutants. Therefore, EXO70C2 may play a role in regulating vesicle secretion during tapetum degeneration process. The pollen exine of *exo70c2* mutants was indistinguishable from wild-type pollen. Thus, the possibility that EXO70C2 regulates vesicles containing precursors such as sporopollenin, the building block of exine, can be ruled out. Instead, EXO70C2 may regulate the tethering of vesicles containing nutrients or lipids needed for pollen

maturation. Previously, a similar pollen abortion phenotype was reported for *lacs1lacs4* mutants that showed a significant reduction in biosynthesis of tryphine lipids required for pollen maturation (Jessen et al. 2011). In addition, *MIA* has been suggested to be involved in the pathway responsible for proper secretion of vesicle cargo to the plasma membrane (Jakobsen et al. 2005). T-DNA insertional mutants of *MIA* suffer from abnormal pollen morphology with severe reduction in fertility (Jakobsen et al. 2005), resembling those of *exo70c2* mutants in this study. Interestingly, microarray analysis of *MIA* mutants indicated that *EXO70C2* is significantly down-regulated (Jakobsen et al. 2005). These data further implies that *MIA* is involved in the secretory pathway, most likely acting upstream of *EXO70C2* to regulate proper secretion of vesicle cargos.

Overall, using TILLING as a reverse genetic approach, I demonstrated the importance of EXO70C2, a subunit of the exocyst complex, in pollen development. This study also suggest that EXO70C2 likely functions in cytokinesis during pollen development through the regulation of secretion of essential vesicles which support pollen maturation. In the future, it will be interesting to analyze in detail the molecular machinery controlling exocyst function in targeted secretion and its possible role in other plant exocytosis processes.

3-5. Figures

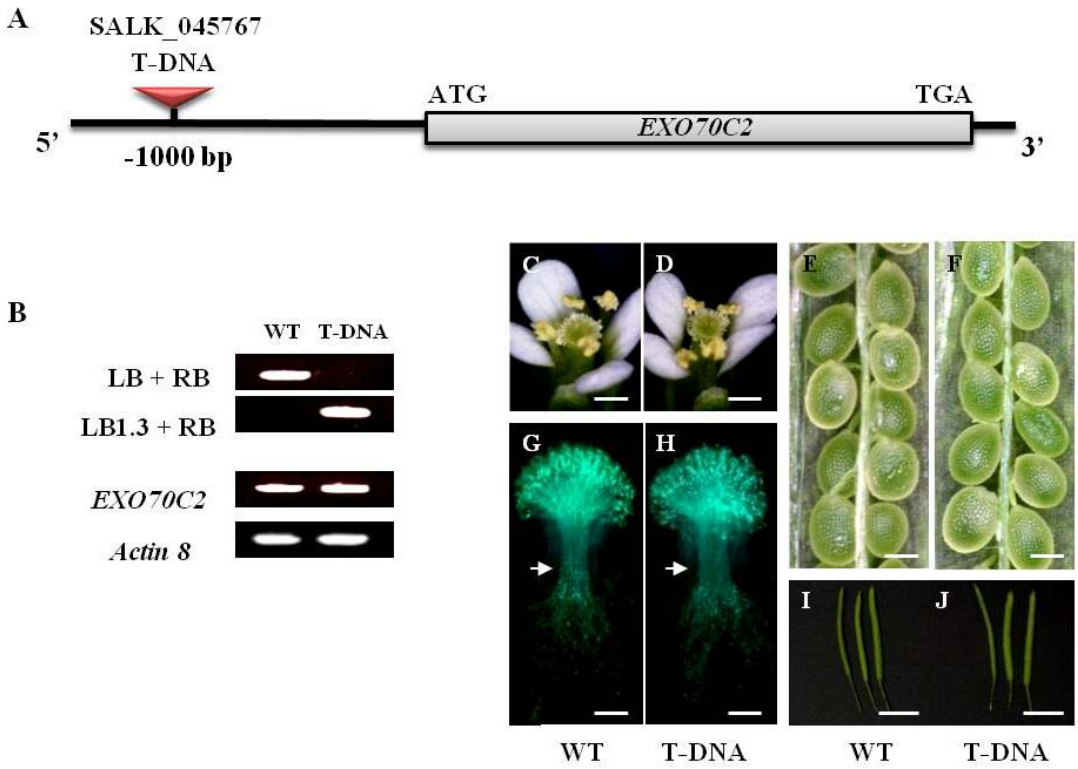

Figure 3-3. Characterization of *EXO70C2* T-DNA insertion line . (A) Schematic view of *EXO70C2* genome structure showing the T-DNA insertion site. (B) Genomic PCR validation (upper panel) and RT-PCR of *EXO70C2* quantification (lower panel) in WT plant (left lane) and homozygous T-DNA insertion line (right lane). LB, LB1.3: left border, RB: right border of T-DNA. Primers specific to *Actin8* were used as internal control. (C-J) Phenotypic characterization of WT plant and *EXO70C2* insertion line. (C, D) Mature flower. (E, F) Seed sets. (G, H) Aniline blue staining of pistils. Pollen tubes are indicated by white arrows. (I, J) Mature siliques. Bars (C), (D), (I), (J): 5 mm, (E) to (H): 500 μm.

A

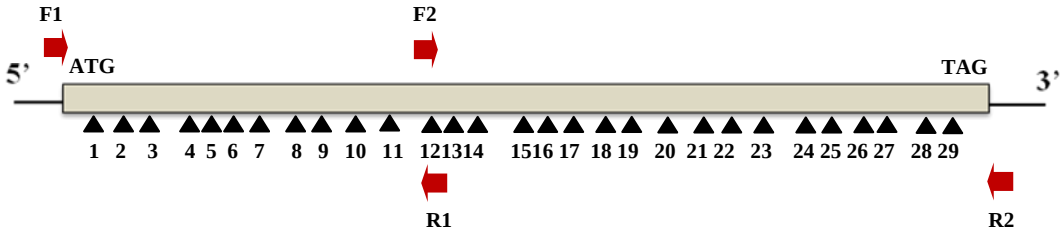

***EXO70C2* (At5g13990)**

No	Position from ATG	Exon/ Intron	Amino acid change	Homo/ Hetero	Mutation type
1	C 220 T (*exo70c2_220*)	Exon	R 74 C	Hetero	Missense
2	G 484 A (*exo70c2_484*)	Exon	G 162 R	Homo	Missense
3	G 544 A (*exo70c2_544/1631*)	Exon	G 182 R	Homo	Missense
4	G 715 A	Exon	D 239 N	Hetero	Missense
5	C 731 T (*exo70c2_731*)	Exon	P 244 L	Homo	Missense
6	C 770 T (*exo70c2_770*)	Exon	P 257 L	Homo	Missense
7	G 802 A (*exo70c2_802*)	Exon	A 268 T	Hetero	Missense
8	G 810 A	Exon	-	Hetero	Sense
9	G 913 A	Exon	V 305 I	Hetero	Missense
10	G 941 A (*exo70c2_941*)	Exon	S 314 N	Homo	Missense
11	G 963 A	Exon	-	Hetero	Sense
12	G 1049 A (*exo70c2_1049*)	Exon	G 350 E	Homo	Missense
13	C 1164 T	Exon	-	Hetero	Sense
14	G 1176 A	Exon	-	Hetero	Sense
15	G 1184 A (*exo70c2_1184*)	Exon	R 395 Q	Hetero	Missense
16	G 1219 A (*exo70c2_1219*)	Exon	E 407 K	Homo	Missense
17	G 1230 A	Exon	-	Hetero	Sense
18	G 1239 A	Exon	-	Hetero	Sense
19	G 1324 A (*exo70c2_1324*)	Exon	D 442 N	Homo	Missense
20	G 1414 A	Exon	D 472 N	Hetero	Missense
21	C 1445 T (*exo70c2_1445*)	Exon	S 482 L	Hetero	Missense
22	G 1481 A (*exo70c2_1481*)	Exon	S 494 N	Homo	Missense
23	C 1497 T	Exon	-	Hetero	Sense

24	G 1534 A	Exon	G 512 R	Hetero	Missense
25	G 1543 A (*exo70c2_1543*)	Exon	E 515 K	Homo	Missense
26	G 1631 A (*exo70c2_554/1631*)	Exon	G 544 E	Hetero	Missense
27	G 1673 A	Exon	R 558 L	Hetero	Missense
28	A 1930 G	Exon	R 644 G	Hetero	Missense
29	G 1952 A	Exon	G 651 E	Hetero	Missense

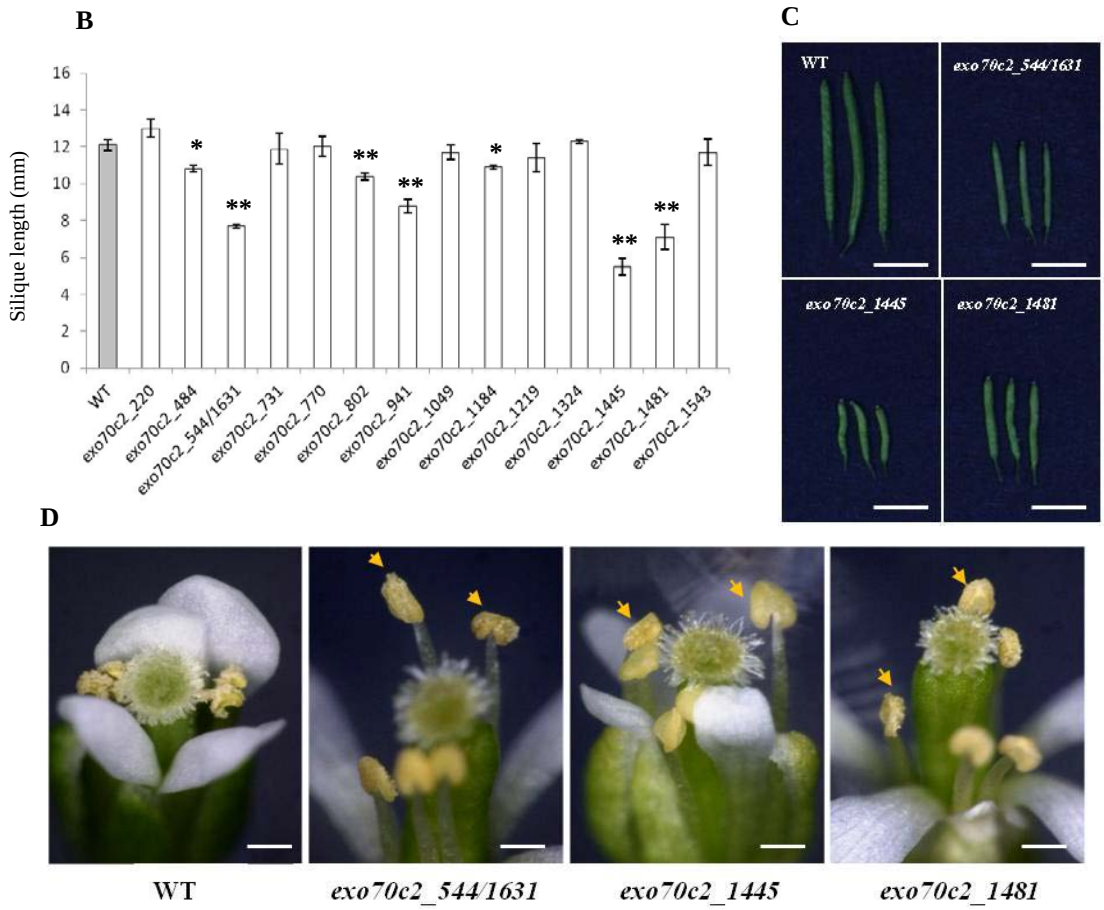

Figure 3-4. Phenotypic analysis of *exo70c2* TILLING mutants. (A) Detailed analysis of mutations found in the *EXO70C2* gene fragment**.** Diagram shows the analysed *EXO70C2* gene fragment and the location of detected mutations (black arrowheads). Forward and reverse primer sites for TILLING analysis are also indicated by red arrows. TILLING mutants selected for silique length measurement are highlighted in blue. TILLING mutant with two point mutations is highlighted in red. (B) Silique length measurement of homozygous *exo70c2* mutants. WT silique was used as control. For each line, 5 siliques were measured for 3 biological replicates. Asterick indicates the *P* values calculated by Student's t-test against WT. * indicates $P < 0.01$, ** indicates $P < 0.005$. (C) Siliques of WT plant and *exo70c2* mutants. (D) Mature flowers of WT plant, *exo70c2_544/1631, exo70c2_1445, and exo70c2_1481* mutants. Anthers with reduced pollen grains are indicated by yellow arrows. Bars: 5 mm

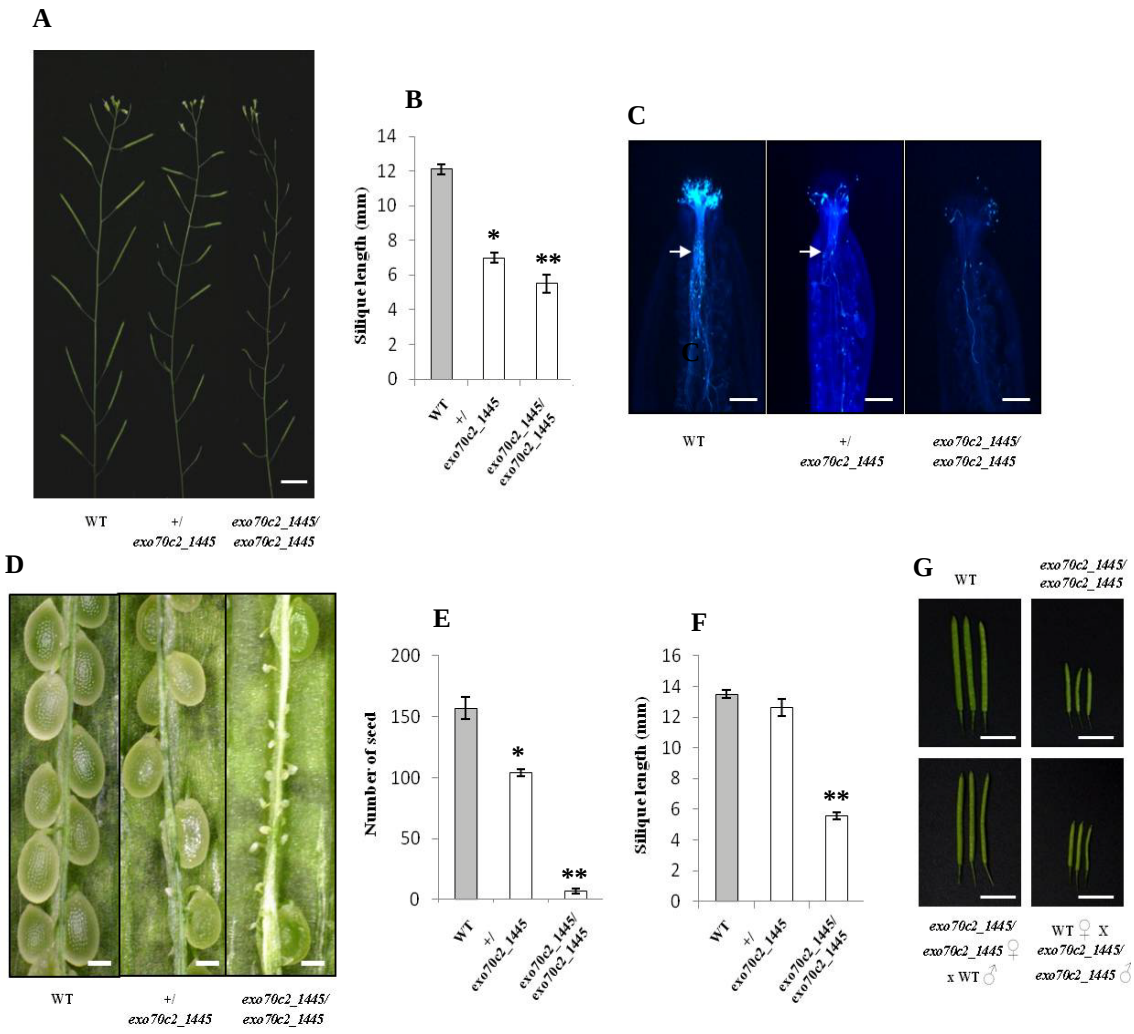

Figure 3-5. Phenotypes of *exo70c2* TILLING mutants. (A) Photograph of seed pods of WT plant (left) and *exo70c2_1445* heterozygous and homozygous mutants (center and right). Bars: 5 mm. (B) Silique length measurement in WT plant and *exo70c2* mutants. For each sample, 5 siliques were measured for 3 biological replicates. (C) Anilline blue staining of pistils from WT plant and *exo70c2* mutants. Pollen tubes are indicated by white arrows. Bars: 200 µm. (D) Seed set of WT plant and *exo70c2* mutants. Bars: 200 µm. (E) Seed count of WT plant and *exo70c2* mutants. For each sample, 5 siliques were counted for 3 biological replicates. (F) Silique length measurement of hand self-pollinated WT and *exo70c2* homozygous mutant lines. (G) Seed pods from self-pollinated (upper panel) and reciprocal cross-pollination (lower panel) of WT and *exo70c2* homozygous mutant line. Bars: 5 mm. Asterick indicates the *P* values calculated by Student's t-test against WT. * indicates $P < 0.01$, ** indicates $P < 0.005$.

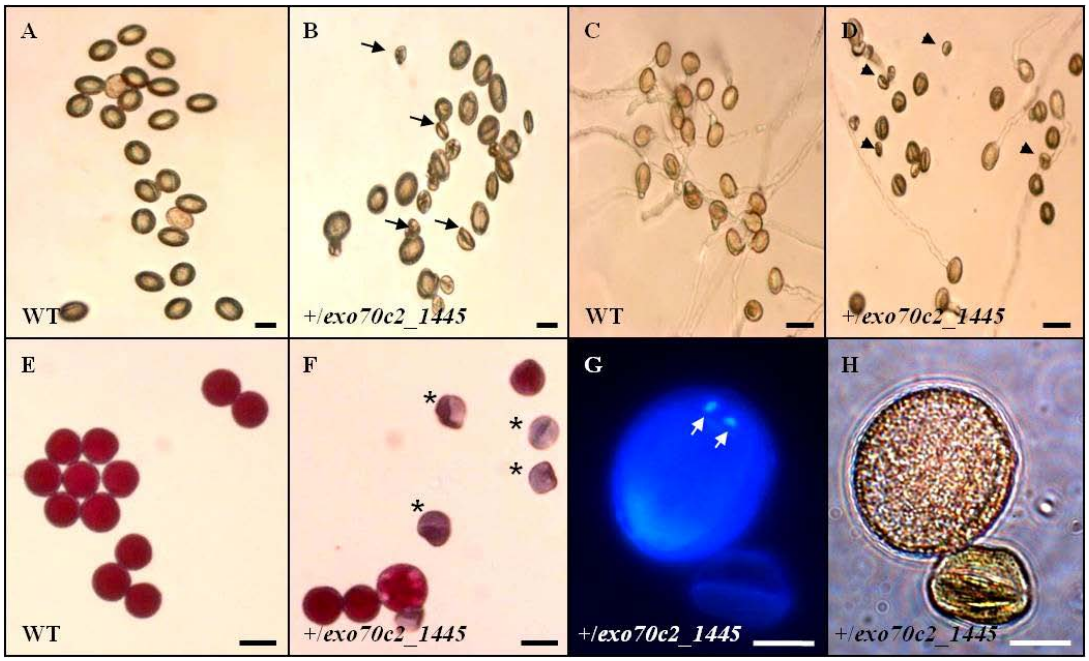

Figure 3-6. Characterization of *exo70c2* mutant pollen. (A), (B) Morphology of pollen grains. Aborted pollen grains are indicated by black arrows (C), (D) Pollen germination and pollen tubes growth. Non-germinated pollen grains are indicated by black arrowheads. (E), (F) Alexander staining of mature pollen grains. Non-viable pollen grains are indicated by astericks. (G), (H) DAPI staining of pollen grains. Sperm cell nuclei are indicated by white arrows. Bars: 10 µm.

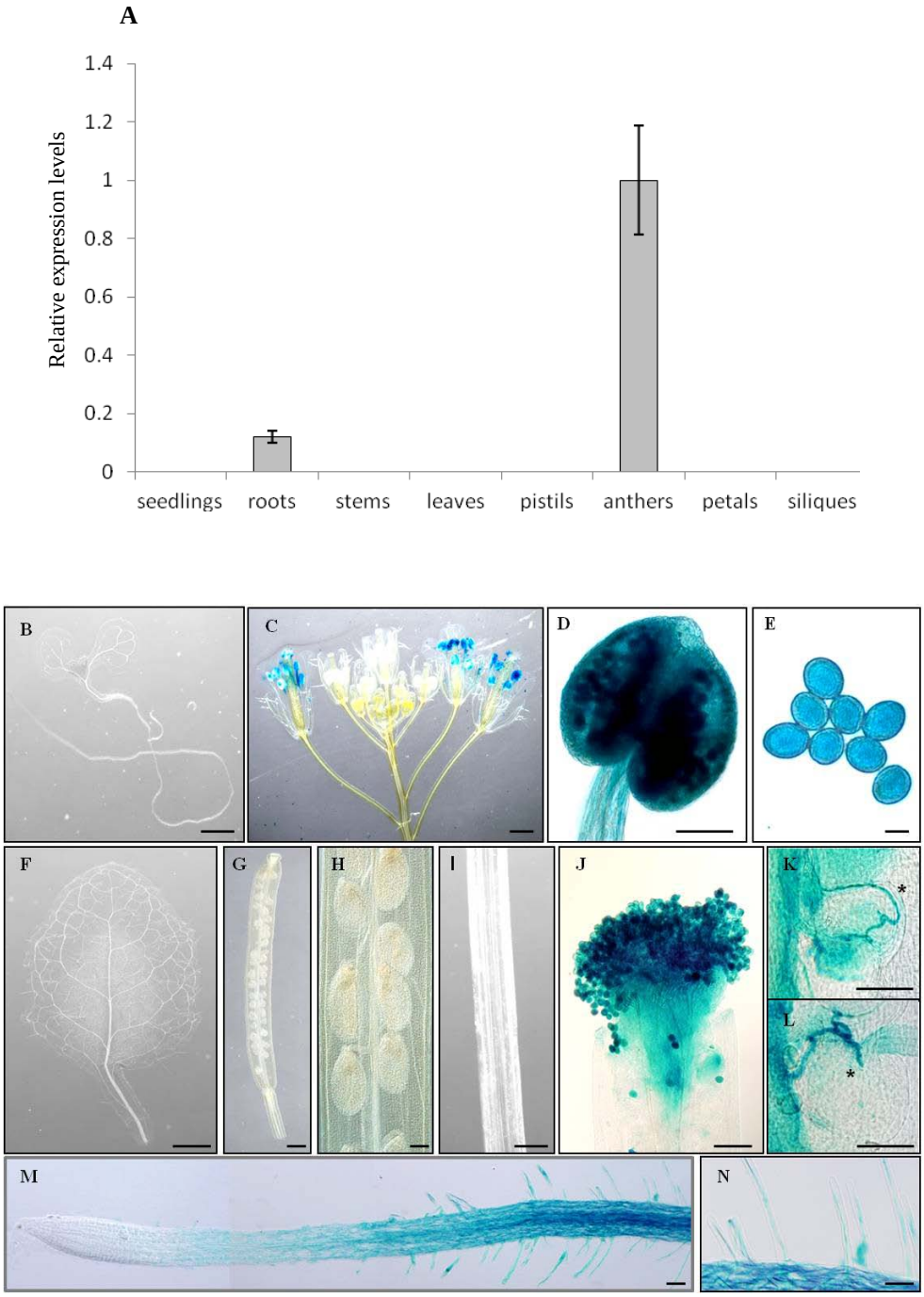

Figure 3-7. *EXO70C2* expression in various *Arabidopsis* tissues. (A) Relative *EXO70C2* expression levels in various tissues, revealed by qRT-PCR (means of three replicates). (B) to (N) Expression pattern of *EXO70C2* revealed by promoter GUS assay in various tissues; (B) 7 days old seedling, (C) inflorescene, (D) anther, (E) mature pollen grains, (F) leave, (G) silique, (H) endosperms, (I) stem, (J) pollinated stigma, (K), (L) pollen tubes penetrating the ovules (*), (M) mature root, (N) root hairs. Bars (B), (D), (F), (H) to (N): 200 µm, (C), (G): 0.5 mm, (E): 10 µm.

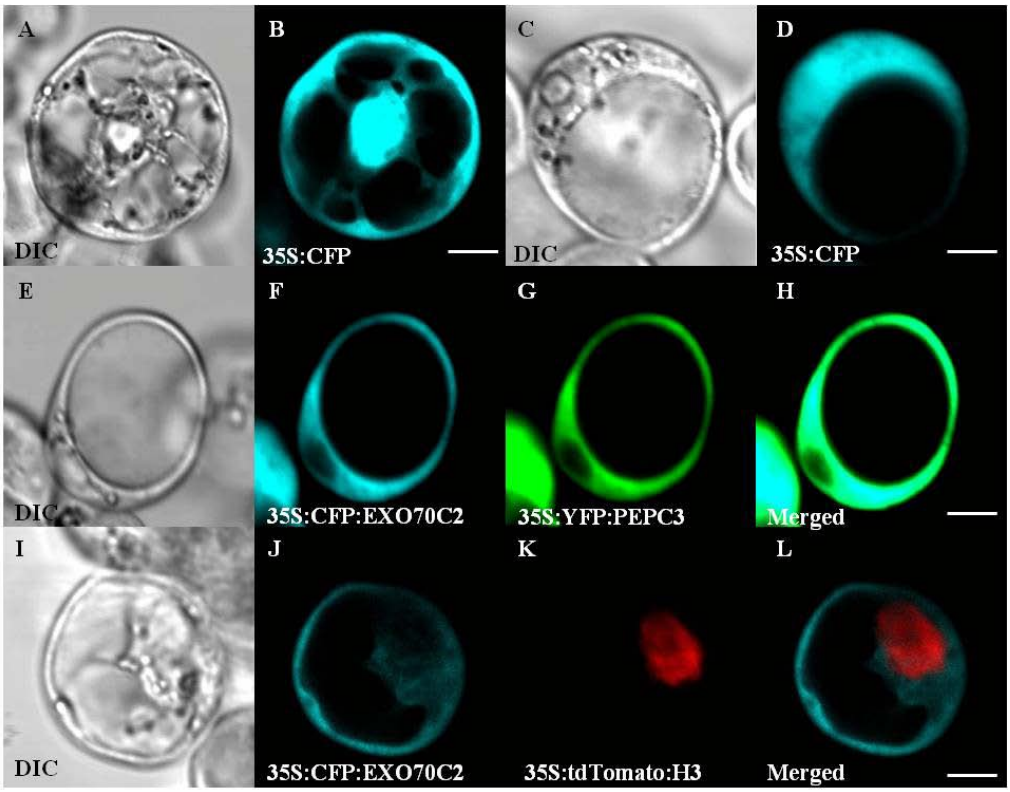

Figure 3-8. Analysis of EXO70C2 subcellular localization. (A) to (D) *Arabidopsis* protoplasts expressing CFP as a control. (E) to (G) *Arabidopsis* protoplast co-expressing CFP:EXO70C2 and YFP:PEPC3. (H) The merged signal of (F) and (G). (I) to (K) *Arabidopsis* protoplast co-expressing CFP:EXO70C2 and tdTomato:H3. (L) The merged signal of (J) and (K). DIC: differential interference contrast. PEP3: phosphoenolpyruvate carboxylase 3 (cytosolic marker). H3: histone H3 (nuclear marker). Bars: 5 µm.

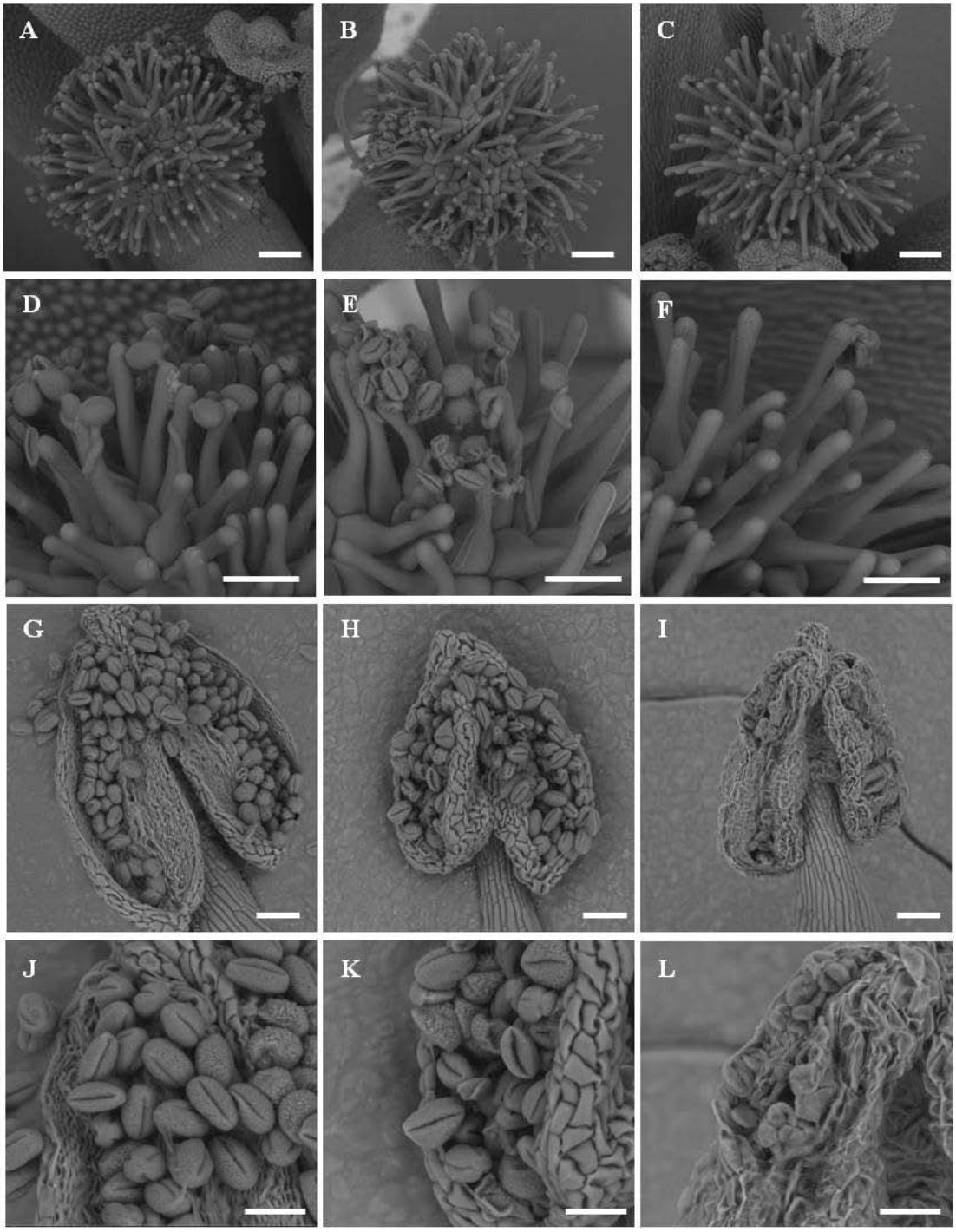

Figure 3-9. Cryo-SEM analysis of anthers, pollen grains and stigmas of WT plant and *exo70c2* mutants. (A) to (C) Stigmas of mature flowers. (D) to (F) Natural self-pollinated papilla cells of mature stigmas. (G) to (L) Anthers of mature flowers. Bars (A) to (C): 100 µm, (D) to (I): 50 µm, (J) to (L): 25 µm.

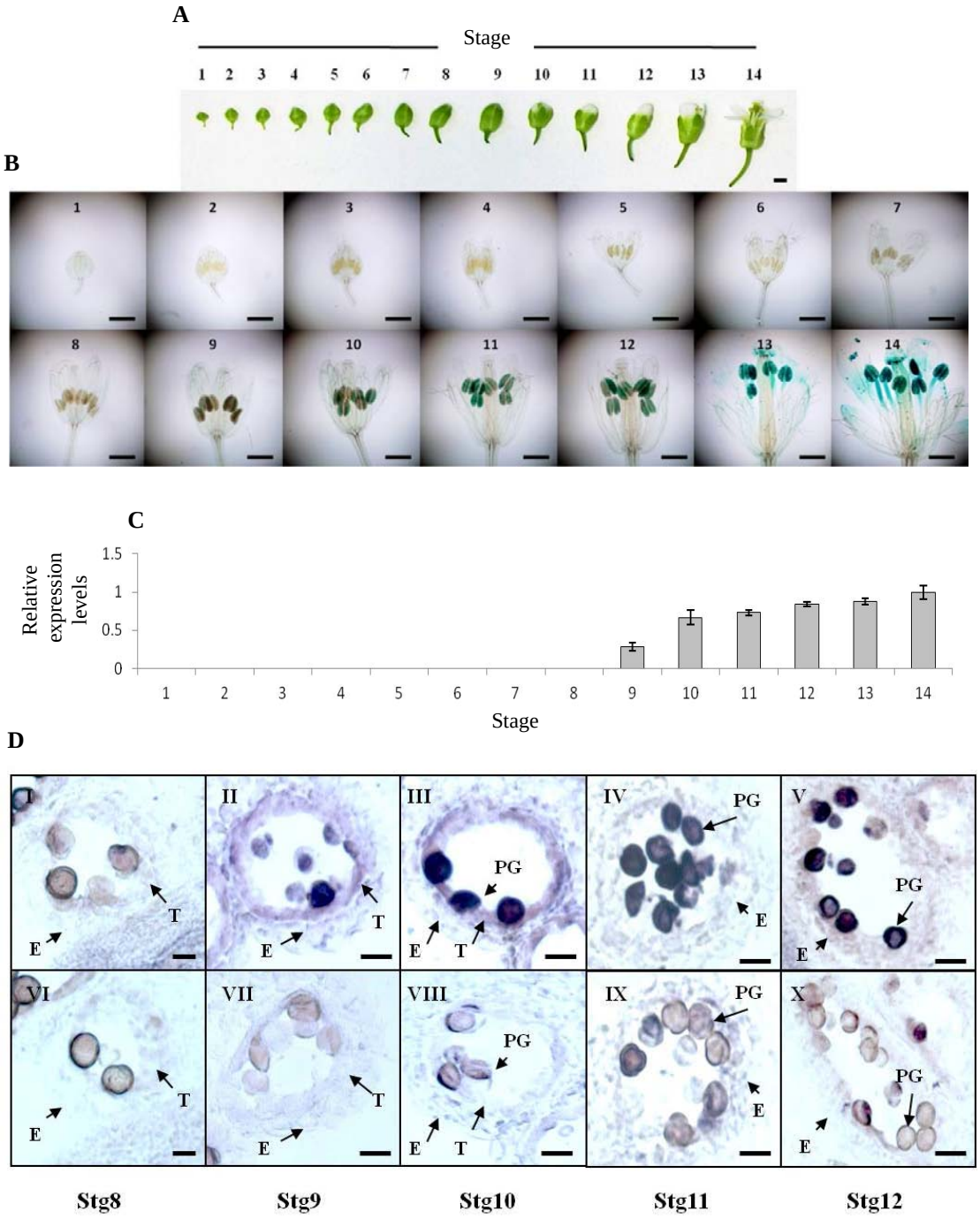

Figure 3-10. Flower buds and *EXO70C2* expression pattern. (A) A series of flower buds during anther development. Bar: 0.5 mm. (B) Expression pattern of *EXO70C2* revealed by GUS assay in various stages of anther development.. Stages of anther development are numbered. Bars: 0.5 mm. (C) qRT-PCR analysis of *EXO70C2*. (D) *In situ* hybridization analyses of *EXO70C2* in wild-type anthers. I to V: probed with labelled *EXO70C2* antisense probe (upper panel). VI to X: probed with excess unlabelled *EXO70C2* antisense probe (lower panel). E: epidermis, PG: pollen grain, Stg: stage, T: tapetum. Bars: 10 μm.

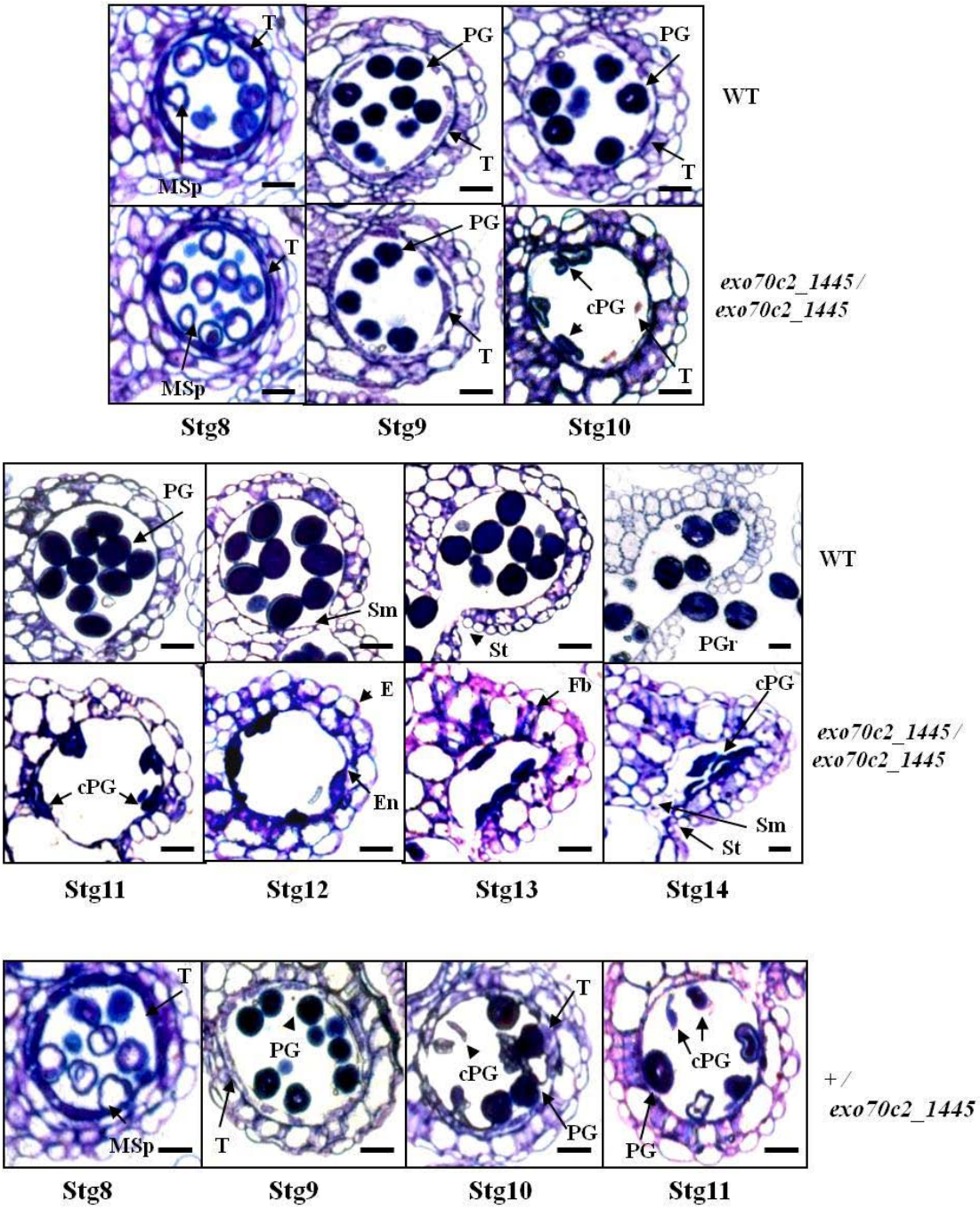

Figure 3-11. Transverse section analysis of the anthers. The toluidine blue stained images were from cross section through a single microsporangium from each stage. cPG: collapsed pollen grains, E : epidermis, En: endothelium, Fb: fibrous bands, MSp: microspore, PG: pollen grains, PGr : pollen grains release, Sm: septum, St: stomium, Stg: stage, T: tapetum. Bars: 10 μm.

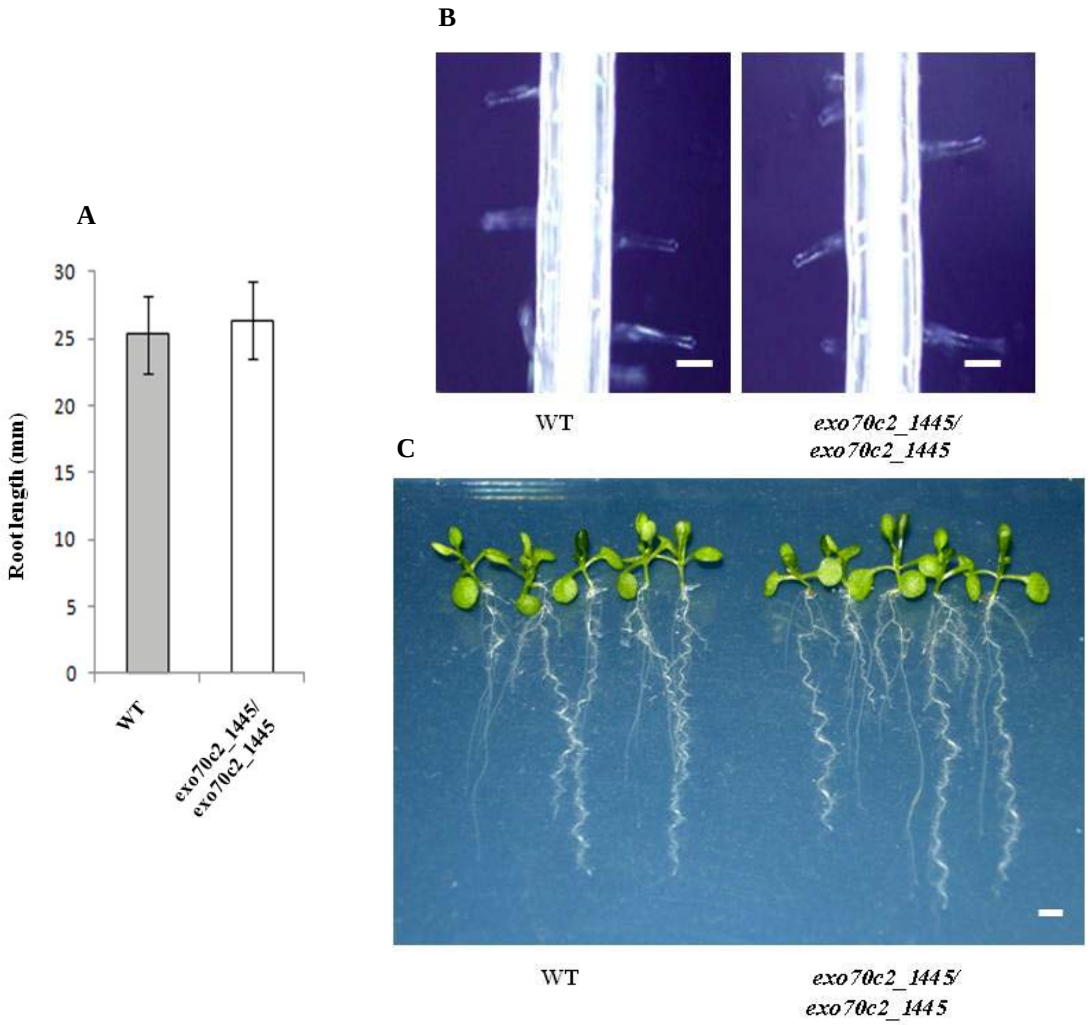

Figure 3-12. Root phenotypic characterization of *exo70c2* mutants. (A) Primary root length measurement after 14 days of growth on 1/2 MS media. For each line, 5 roots were measured for 3 biological replicates. (B) Primary root and root hairs of WT plant and *exo70c2* mutant. Bars: 200 µm. (C) Photograph of 14 days old seedlings used for root phenotypic characterization. Bars: 5 mm.

Acknowledgements

First and foremost, I would like to express my sincere gratitude to my supervisor Prof. Seiji Takayama for his guidance, encouragement, and patience during my four years stay in Intercellular Communications Laboratory. I also thank Ass. Prof. Megumi Iwano, Dr. Pulla Kathioen-Nakayama, and Dr. Tetsuyuki Entani for their guidance and help over the years. I am grateful to Yuka Yamamoto and Saori Higo for excellent technical assistance. My sincere appreciation is also express to my committee members; Prof. Ko Shimamoto, Prof. Takashi Hashimoto, and Assoc. Prof. Miyo Morita for their time, interest, and constructive comments.

Also, thanks to all my lab members and friends at NAIST for their support and help. I gratefully acknowledge the funding sources from NAIST Global COE program that made my Ph.D. study possible. Last but not least, I would like to express my deepest appreciation to my family for their encouragement and love.

References

AGI: Analysis of the genome sequence of the flowering plant *Arabidopsis thaliana*. (2000). Nature 408, 796-815.

Alexander, M.P. (1969). Differential staining of aborted and nonaborted pollen. Stain Technol. 44, 117-122.

Alonso, J.M., Stepanova, A.N., Leisse, T.J., Kim, C.J., Chen, H., Shinn, P., Stevenson, D.K., Zimmerman, J., Barajas, P., Cheuk, R., Gadrinab, C., Heller, C., Jeske, A., Koesema, E., Meyers, C.C., Parker, H., Prednis, L., Ansari, Y., Choy, N., Deen, H., Geralt, M., Hazari, N., Hom, E., Karnes, M., Mulholland, C., Ndubaku, R., Schmidt, I., Guzman, P., Aguilar-Henonin, L., Schmid, M., Weigel, D., Carter, D.E., Marchand, T., Risseeuw, E., Brogden, D., Zeko, A., Crosby, W.L., Berry, C.C., and Ecker, J.R. (2003). Genome-wide insertional mutagenesis of *Arabidopsis thaliana*. Science 301, 653-657.

Antunes, M.S., Morey, K.J., Tewari-Singh, N., Bowen, T.A., Smith, J.J., Webb, C.T., Helinga, H.W., and Medford, J.L. (2009). Engineering key components in a synthetic eukaryotic signal transduction pathway. Mol. Syst. Biol. 5, 270.

Barth, S., Melchinger, A.E., and Lubberstedt, T. (2002). Genetic diversity in *Arabidopsis thaliana* L. Heynh. investigated by cleaved amplified polymorphic sequences (CAPS) and inter-simple sequence repeat (ISSR) markers. Mol. Ecol. 11, 495-505.

Bechtold, U., Lawson, T., Mejia-Carranza, J., Meyer, R.C., Brown, I.R., Altman, T., Ton, J., and Mullineaux, P.M. (2010). Constitutive salicylic acid defences do not compromise seed yield, drought tolerance and water productivity in *Arabidopsis* accession C24. Plant Cell Environ. 33, 1959-1973.

Brosche, M., Merilo, E., Mayer, F., Pechter, P., Puzõrjova, I., Brader, G., Kangasjärvi, J., and Kollist, H. (2010). Natural variation in ozone sensitivity among *Arabidopsis thaliana* accessions and its relation to stomatal conductance. Plant Cell Environ. 33, 914-925.

Chong, Y.T., Gidda, S.K., Sanford, C., Parkinson, J., Mullen, R.T., and Goring, D.R. (2010). Characterization of the *Arabidopsis thaliana* exocyst complex gene families by phylogenetic, expression profiling, and subcellular localization studies. New Phytol. 185, 401-419.

Clough, S.J., and Bent, A.F. (1998). Floral dip: a simplified method for Agrobacterium-mediated transformation of *Arabidopsis thaliana*. Plant J. 16, 735-743.

Cole, R.A., and Fowler, J.E. (2006). Polarized growth: maintaining focus on the tip. Curr. Opin. Plant Biol. 9, 579-588.

Cole, R.A., Synek, L., Zarsky, V., and Fowler, J.E. (2005). SEC8, a subunit of the putative *Arabidopsis* exocyst complex, facilitates pollen germination and competitive pollen tube growth. Plant Physiol. 138, 2005-2018.

Crowell, E.F., Bischoff, V., desprez, T., Rolland, A., Stierhof, Y.D., Schumacher, K., Gonneau, M., Hofte, H., and Vernhettes, S. (2009). Pausing of Golgi bodies on microtubules regulates secretion of cellulose synthase complexes in *Arabidopsis*. Plant Cell 21, 1141-1154.

Dobbelaere, J., and Barral, Y. (2004). Spatial coordination of cytokinetic events by compartmentalization of the cell cortex. Science 305, 393-396.

Ellis, C., Karafyllidis, I., Wasternack, C., and Turner, J.G. (2002). The *Arabidopsis* mutant cev1 links cell wall signaling to jasmonate and ethylene responses. Plant Cell 14**,** 1557–1566.

Emons, A.M.C., and Ketelaar, T. (2009). Root hairs. Plant cell monographs series, Vol 12, Springer, Berlin.

Fendrych, M., Synek, L., Pecenkova, T., Toupaluva, H., Cole, R., Drdova, E., Nebesarova, J., Sedinova, M., Hala, M., and Fowler, J.E. (2010). The *Arabidopsis* complex is involve in cytokinesis and cell plate maturation. Plant Cell 22, 3053-3065.

Fielding, A.B., Schonteich, E., Matheson, J., Wilson, G., Yu, X., Hickson, G.R.X., Srivastava, S., Baldwin, S.A., Prekeris, R., and Gould, G.W. (2005). Rab11-FIP3 and FIP4 interact with Arf6 and the exocyst to control membrane traffic in cytokinesis. EMBO J. 24, 3389-3399.

González, M., Xu, M., Esteras, C., Roig, C., Monforte, A.J., Troadec, C., Pujol, M., Nuez, F., Bendahmane, A., Garcia-Mas, J., and Picó, B. (2011). Towards a TILLING platform for functional genomics in Piel de Sapo melons. BMC Res. Notes 4, 289.

Greene, E.A., Codomo, C.A., Taylor, N.E., Henikoff, J.G., Till, B.J., Reynolds, S.H., Enns, L.C., Burtner, C., Johnson, J.E., Odden, A.R., Comai, L., and Henikoff, S. (2003). Spectrum of chemically induced mutations from a large-scale reverse genetic screen in *Arabidopsis*. Genetics 164, 731-740.

Gromley, A., Yeaman, C., Rosa, J., Redick, S., Chen, C.T., Mirabelle, S., Guha, M., Sillibourne, J., and Doxsey, S.J. (2005). Centriolin anchoring of exocyst and SNARE complexes at the midbody is required for secretory-vesicle-mediated abscission. Cell 123, 75-87.

Guertin, D.A., Trautmann, S., and McCollum, D. (2002). Cytokinesis in eukaryotes. Microbiol. Mol. Biol. Rev. 66, 155-178.

Gutierrez, R., Lindeboom, J.J., Paredez, A.R., Emons, A.M.C., and Ehrhardt, D.W. (2009). *Arabidopsis* cortical microtubules position cellulose synthase delivery to the plasma membrane and interact with cellulose synthase trafficking compartments. Nat. Cell. Biol. 11, 797-806.

Guo, W., Grant, A., and Novick, P. (1999). Exo84p is an exocyst protein essential for secretion. J. Biol. Chem. 274, 23558-23564.

Hála, M., Cole, R., Synek, L., Drdová, E., Pečenková, T., Nordheim, A., Lamkemeyer, T., Madlug, J., Hochholdinger, F., Fowler, E.J., and Žarský, V. (2008). An exocyst complex functions in plant cell growth in *Arabidopsis* and tobacco. Plant Cell 20, 1330-1345.

He, B., Xi, F., Zhang, H., Zhang, J., and Guo, W. (2007). Exo70 interacts with phospholipids and mediates the targeting of the exocyst to the plasma membrane. EMBO J. 26, 4053-4065.

Henikoff, S., Till, B.J., and Comai, L. (2004). TILLING: traditional mutagenesis meets functional genomics. Plant Physiol. 135, 630-636.

Hsu, S.C., TerBush, D., Abraham, M., and Guo, W. (2004). The exocyst complex in polarized exocytosis. Int. Rev. Cytol. 233, 243-265.

Jakobsen, M.K., Poulsen, L.R., Schulz, A., Fleurat-lessard, P., Moller, A., Husted, S., Schiott, M., Amtmann, A., and Palmgren, M.G. (2005). Pollen development and fertilization in *Arabidopsis* is dependent on the *MALE GAMETOGENESIS IMPAIRED ANTHERS* gene encoding Type V P-type ATPase. Ganes Dev. 19, 2757-2769.

Jander, G., Norris, S.R., Rounsley, S.D., Bush, D.F., Levin, I.M., and Last, R.L. (2002). *Arabidopsis* map-based cloning in the post-genome era. Plant Physiol. 129, 440-450.

Jefferson, R.A., Kavanagh, T.A., and Bevan, M.W. (1987). GUS fusion: β-glucuronidase as a sensitive and versatile gene fusion marker in higher plants. EMBO J. 6, 3901-3907.

Jessen, D., Olbrich, A., Knufer, J., Kruger, A., Hoppert, M., Polle, A., and Fulda, M. (2011). Combined activity of *LACS1* and *LACS4* is required for proper pollen coat formation in *Arabidopsis*. Plant J. 68, 715-726.

Kanathani, A. (2008). アブラナ科植物の自家不和合性における情報伝達系の解析. NAIST, Master Thesis Dissertation.

Kakita, M., Murase, K., Iwano, M., Matsumoto, T., Watanabe, M., Shiba, H., Isogai, A., and Takayama, S. (2007). Two distinct forms of M-locus protein kinase localize to the plasma membrane and intercat directly with S-locus receptor kinase to transduce self-incompatibility signalling in *Brassica rapa*. Plant Cell 19, 3961-3973.

Karssen, C.M., Brinkhorst-van der Swan, D.L.C., Breekland, A.E., and Koornneef, M. (1983). Induction of dormancy during seed development by endogenous abscisic acid: studies on abscisic acid deficient genotypes of *Arabidopsis thaliana* (L.) Heynh. Planta 157, 158-165.

Kim, Y., Schumaker, K.S., and Zhu, J.K. (2006). EMS mutagenesis of *Arabidopsis*. Methods Mol. Biol. 323, 101-103.

Kitashiba, H., Liu, P., Nishio, T., Nasrallah, J.B., and Nasrallah, M.E. (2011). Functional test of Brassica self-incompatibility modifiers in *Arabidopsis thaliana*. PNAS 108, 18173-19178.

Koch, M.A., Houbold, B., and Michell-Olds, T. (2001). Molecular systematics of the Brassicaceae: Eevidence from coding plastidic *matK* and nuclear *Chs* sequences. Am. J. Bot. 88, 534-544.

Koornneef, M., Jorna, M.L., Brinkhorst-van der Swan, D.L.C., and Karssen, C.M. (1982). The isolation of abscisic acid (ABA) deficient mutants by selection of induced revertants in non-germinating gibberellin sensitive lines of *Arabidopsis thaliana* (L.) Henyh. Theor. Appl. Genet. 61, 385-393.

Kulich, I., Cole, R., Drdova, E., Cvrckova, F., Soukup, A., Fowler, J., and Zarsky, V. (2010). *Arabidopsis* exocyst subunits SEC8 and EXO70A1 and exocyst interactor ROH1 are involved in the localized deposition of seed coat pectin. New Phytol. 188, 615-625.

Kurowska, M., Daszkowska-Golec, A., Gruszka, D., Marzec, M., Szurman, M., Szarejko, I., and Maluszynski. (2011). TILLING – a shortcut in functional genomics. J. Appl. Genet. 52, 371-390.

Lai, K.S., Kathoien-Nakayama, P., Iwano, M., and Takayama, S. A TILLING resource for functional genomics in Arabidopsis thaliana accession C24. Genes Genet. Syst. (in press)

Lam, S.H., Lee, S.G., Lin, C.Y., Thomsen, J.S., Fu, P.Y., Murthy, K.R., Li, H., Govindarajan, K.R., Nick, l.C., Bourque, G., Gong, Z., Lufkin, T., Liu, T., and Mathavan, S. (2011). Molecular conservation of estrogen-response associated with cell cycle regulation, hormonal carcinogenesis and cancer in zebrafish and human cancer cell lines. BMC Med. Genomics 4, 41.

Langdale, J.A. (1994). *In situ* hybridization. In The Maize Handbook. New York: springer-Verlag, 165-180.

Lavy, M., Bloch, D., Hazak, O., Gutman, I., Poraty, L., Sorek, N., Sternberg, H., and Yalovsky, S.A. (2007). Novel ROP/Rac effector links cell polarity, root-meristem maintenance, and vesicle trafficking. Curr. Biol. 17, 947-952.

Li, S., Gwen, M.A.V., Ren, S., Yu, D., Ketelaar, T., Emons, A.M.C., and Liu, C.M. (2010). Expression and functional analyses of EXO70 genes in *Arabidopsis* implicate roles in regulating cell type-specific exocytosis. Plant Physiol. 154, 1819-1830.

Li, X., Song, Y., Century, K., Straight, S., Ronald, P., Dong, X., Lassner, M., and Zhang, Y. (2001). A fast neutron deletion mutagenesis-based reverse genetics system for plants. Plant J. 27, 235-242.

Malamy, J.E., and Benfey, P.N. (1997). Organization and cell differentiation in lateral roots of *Arabidopsis thaliana*. Development 124, 33-44.

Martín, B., Ramiro, M., Martínez-Zapater, J.M., and Alonso-Blanco, C. (2009). A high-density collection of EMS-induced mutations for TILLING in Landsberg *erecta* genetic background of *Arabidopsis*. BMC Plant Biol. 9, 147.

Matern, H.T., Yeaman, C., Nelson, W.J., and Scheller, R.H. (2001). The Sec6/8 complex in mammalian cells: characterization of mammalian Sec3, subunit interactions, and expression of subunits in polarized cells. Proc. Natl. Acad. Sci. USA 98, 9648-9653.

McCallum, C.M., Comai, L., Greene, E.A., and Henikoff, S. (2000). Targeted screening for induced mutations. Nat. Biotechnol. 18, 455-457.

McCallum, C.M., Comai, L., Greene, E.A., and Henikoff, S. (2000). Targeted screening for induced mutations. Nat. Biotechnol. 18, 455-457.

Miki, D., and Shimamoto, K. (2004). Simple RNAi vectors for stable and transient suppression of gene function in rice. Plant and Cell Physiol. 45, 490-495.

Miller, D.D., de Ruijter, N.C.A., and Emons, A.M.C. (1997). From signal to form: aspects of the cytoskeleton-plasma membrane-cell wall continuum in root hair tips. J. Exp. Bot. 48, 1881-1896.

Minioa, S., Petrozza, A., D'Onofrio, O., Piron, F., Mosca, G., Sozio, G., cellini, F., Bendahmane, A., and Carriero, F. (2010). A new mutant genetic resource for tomato crop improvement by TILLING technology. BMC Res. Notes 3, 69.

Munson, M., and Novick, P. (2006). The exocyst defrocked, a framework of rods revealed. Nat. Struc. Mol. Biol. 13, 577-581.

Murgia, M., Charzynska, M., Rougier, M., and Cresti, M. (1991). Secretory tapetum of *Brassica oleracea* L.: polarity and ultrastructural features. Sex. Plant Reprod. 4, 28-35.

Nasrallah, M.E., Liu, P., and Nasrallah, J.B. (2002). Generation of self-incompatible *Arabidopsis thaliana* by transfer of two *S* locus genes from *A. lyrata*. Science 297, 247-249.

Ng, P.C., and Henikoff, S. (2003). SIFT: predicting amino acid changes that affect protein function. Nucleic Acids Res. 31, 3812-3814.

Otegui, M.S., and Staehelin, L.A. (2004). Electron tomographic analysis of post-meiotic cytokinesis during pollen develpment in *Arabidopsis thaliana*. Planta 218, 501-515.

Otegui, M.S., Verbrugghe, K.J., and Skop, A.R. (2005). Midbodies and phragmoplasts: Analogous structures involved in cytokinesis. Trends Cell Biol. 15, 404-413.

Park, S.K., Howden, R., and Twell, D. (1998). The *Arabidopsis thaliana* gametophytic mutation gemini pollen 1 disrupts microspore polarity, division asymmetry and pollen cell fate. Development 125, 3789–3799.

Pecenkova, T., Hala, M., Kulich, I., Kocourkova, D., Drdova, E., Fendrych, M., Toupalova, H., and Zarsky, V. (2011). The role for the exocyst complex subunits EXO70B2 and EXO70H1 in the plant-pathogen interaction. J. Exp. Bot. 62, 2107-2116.

Perry, J., Brachmann, A., Welham, T., Binder, A., Charpentier, M., Groth, M., Haage, K., Markmann, K., Wang, T.L., and Parniske, M. (2009). TILLING in Lotus japonica identified large allelic series for symbiosis genes and revealed a bias in functionally defective ethyl methanesulfonate alleles toward glycine replacements. Plant Physiol. 151, 1281-1291.

Rea, A.C., Liu, P., and Nasrallah, J.B. (2010). A transgenic self-incompatible *Arabidopsis thaliana* model for evolutionary and mechanistic studies of crucifer self-incompatibility. J. Exp. Bot. 61, 1897-1906.

Rohde, P., Hincha, D.K., and Heyer, A.G. (2004). Heterosis in the freezing tolerance of crosses between two *Arabidopsis thaliana* accessions (Columbia-O and C24) that show differences in non-acclimated and acclimated freezing tolerance. Plant J. 38, 290-299.

Rotman, N., Durbarry, A., Wardle, A., Yang, W.C., Chaboud, A., Faure, J.E., Berger, F., and Twell, D. (2005). A novel class of MYB factors controls sperm-cell formation in plants. Curr. Biol. 15, 244-248.

Rotman, N., Rozier, F., Boavida, L., Dumas, C., Berger, F., and Faure, J.E. (2003). Female control of male gamete delivery during fertilization in *Arabidopsis thaliana*. Curr. Biol. 13, 432–436.

Samuel, M.A., Chong, Y.T., Haasen, K.E., Aldea-Brydges, M.G., Stone, S.L., and Goring, D.R. (2009). Cellular pathways regulating responses to compatible and self-incompatible pollen in *Brassica* and *Arabidopsis* stigmas intersect at EXO70A1, a putative component of exocyst complex. Plant Cell 21, 2655-2671.

Sanders, P.M., Bui, A.Q., Weterings, K., McIntire, K.N., Hsu, Y.C., Lee, P.Y., Truong, M.T., Beals, T.P., and Goldberg, R.B. (1999). Anther developmental defects in *Arabidopsis thaliana* male-sterile mutants. Sex. Plant Reprod. 11, 297-322.

Schneeberger, K., Ossowki, S., Ott, F., Klein, J.D., Wang, X., Lanz, C., Smith, L.M., Cao, J., Fitz, J., Warthmann, N., Henz, S.R., Huson, D.H., and Weigel, D. (2011). Reference-guided assembly of four diverse *Arabidopsis thaliana* genomes. PNAS 108, 10249-10254.

Scott, J.R., Spielman, M., and Dickinson, H.G. (2004). Stamen structure and function. Plant Cell 16, S46-S60.

Segui-Simarro, J.M., Austin II, J.R.I.I., White, E.A., and Staehelin, L.A. (2004). Electron tomographic analysis of somatic cell plate formation in meristematic cells of *Arabidopsis* preserved by high-pressure freezing. Plant Cell 16, 836-856.

Shiu, S.H., and Bleecker, A. B. (2003). Expansion of the receptor-like kinase/Pelle gene family and receptor-like proteins in *Arabidopsis*. Plant Physiol 132, 530-543.

Songer, J.A., and Munson, M. (2009). Sec6p anchors the assembled exocyst complex at sites of secretion. Mol. Biol. Cell 20, 973-982.

Sumie, I., Akiko, K., Junichi, U., Ikuo, N., and Kiyotaka, O. (2001). The DEFECTIVE IN ANTHER DEHISCENCE1 gene encodes a novel phospholipase A1 catalyzing the initial step of jasmonic acid biosynthesis, which synchronizes pollen maturation, anther dehiscence, and flower opening in *Arabidopsis*. Plant Cell 10, 2191–2210.

Synek, L., Schlager, N., Elias, M., Quentin, M., Hausser, M.T., and Zarsky, V. (2006). At EXO70A1, a member of a family of putative exocyst subunits specifically expanded in land plants, is important for polar growth and plant development. Plant J. 48, 54-72.

Sztul, E., and Lupashin, V. (2006). Role of tethering factors in secretory membrane traffic. Am. J. Physiol. Cell Physiol. 290, C11-C26.

Takayama, S., and Isogai, A. (2005). Self-incompatibility in plants. Annu. Rev. Plant. Biol. 56, 467-489.

Till, B.J., Cooper, J., Tai, T.H., Colowit, P., Greene, E.A., Henikoff, S., and Comai, L. (2007). Discovery of chemically induced mutations in rice by TILLING. BMC Plant Biol. 7, 19.

Till, B.J., Reynolds, S.H., Greene, E.A., Codomo, C.A., Enns, L.C., Johnson, J.E., Burtner, C., Odden, A.R., Young, K., Taylor, N.E., Henikoff, J.G., Comai, L., and Henikoff, S. (2003). Large-scale discovery of induced point mutations with high-throughput TILLING. Genome Res. 13, 524-530.

Till, B.J., Reynolds, S.H., Weil, C., Springer, N., Burtner, C., Young, K., Bowers, E., Codomo, C.A., Enns, L.C., Odden, A.R., Greene, E.A., Comai, L., and Henikoff, S. (2004). Discovery of induced point mutations in maize genes by TILLING. BMC Plant Biol. 4, 12.

Till, B.J., Zerr, T., Comai, L., amd Henikoff, S. (2006). A protocol for TILLING and Ecotilling in plants and animals. Nat. Protoc. 1, 2465-2477.

Törjek, O., Berger, D., Meyer, R.C., Müssig, C., Schmid, K.J., Rosleff, S.T., Weisshaar, B., Mitchell-Olds, T., and Altmann, T. (2003). Establishment of a high-efficiency SNP-based framework set for *Arabidopsis*. Plant J. 36, 122-140.

Tsuboi, T., Ravier, M.A., Xie, H., Ewart, M.A., Gould, G.W., Baldwin, S.A., and Rutter, G.A. (2005). Mammalian exocyts complex is required for the docking step of insulin vesicle exocytosis. J. Biol. Chem. 280, 25565-25570.

Verplank, L., and Li, R. (2005). Cell cycle-regulated trafficking of Chs2 controls actomyosin ring stability during cytokinesis. Mol. Biol. Cell 16, 2529-2543.

Vizcay-Barrena, G., and Wilson, Z.A. (2006). Altered tapetal PCD and pollen wall development in the *Arabidopsis ms1* mutant. J. Exp. Bot. 57, 2709-2717.

Wang, N., Wang, Y., Tian, F., King, G.J., Zhang, C., Long, Y., Shi, L., and Meng, J. (2008). A functional genomics resource for *Brassica napus*: development of an EMS mutagenized population and discovery of *FAE1* point mutations by TILLING. New Phytol. 180, 751-765.

Wen, T.J., Hochholdinger, F., Sauer, M., Bruce, W., and Schnable, P.S. (2005). The roothairless 1 gene of maize encodes a homolog of sce3, which involved in polar exocytosis. Plant Physiol. 138, 1637-1643.

Wienholds, E., van Eeden, F., Kosters, M., Muddle, J., Plasterk, R.H.A., and Cuppen, E. (2003). Efficient target-selected mutagenesis in zebrafish. Genome Res. 13, 2700-2707.

Wilson, Z.A., and Zhang, D.B. (2009). From *Arabidopsis* to rice: pathways in pollen development. J. Exp. Bot. 60, 1479-1492.

Winkler, S., Schwabedissen, A., Backasch, D., Bökel, C., Seidel, C., Bönisch, S., Fürthauer, M., Kuhrs, A., Cobreros, L., Brand, M., and González-Gaitán, M. (2005). Target-selected mutant screen by TILLING in *Drosophilla*. Genome Res. 15, 718-723.

Wisman, E., Hartmann, U., Sagasser, M., Baumann, E., Palme, K., Hahlbrock, K., Saedler, H., and Weisshaar. E. (1998). Knock-out mutants from an En-1 mutagenized *Arabidopsis thaliana* population generate phenylpropanoid biosynthesis phenotypes. PNAS 95, 12432-12437.

Xu, L., Liu, F., Lechner, E., Genschik, P., Crosby, W.L., Ma, H., Peng, W., Huang, D., and Xie, D. (2002). The SCF^{COI1} ubiquitin-ligase complexes are required for jasmonate response in *Arabidopsis*. Plant Cell 14, 1919-1935.

Xue, T., Wang, D., Zhang, S., Ehlting, J., Ni, F., Jakab, S., Zheng, C., and Zhong, Y. (2008). Genome-wide and expression analysis of protein phosphates 2C in rice and *Arabidopsis*. BMC Genomics 9, 550.

Yang, Y.W., Lai, K.N., Tai, P.Y., and Li, W.H. (1999). Rates of nucleotide substitution in angiosperm mitochondria DNA sequences and dates of divergence between *Brassica* and other angiosperms lineages. J. Mol. Evol. 48, 597-604.

Yang, Z. (1998). Signalling tip growth in plants. Curr. Opin. Plant Biol. 1, 525-530.

Yoo, S.D., Cho, Y.H., and Sheen, J. (2007). *Arabidopsis* mesophyll protoplasts: a versatile cell system for transient gene expression analysis. Nat. Protoc. 2, 1565-1572.

Zarsky, V., Cvrckova, F., Potocky, M., and Hala, M. (2009). Exocytosis and cell polarity in plants-exocyts and recycling domains. New Phytol. 183, 255-272.

Zhang, Y., Liu, C.M., Emons, AM.C,, and Ketelaar, T. (2010). The plant exocyst. J. Integr. Plant Biol. 52, 138-146.

Zheng, Z., Xia, Qun., Dauk, M., Shen, W., Selvaraj, G., and Zou, J. (2003) *Arabidopsis AtGPAT1*, a member of the membrane-bound glycerol-3-phosphate acyltransferase gene family, is essential for tapetum differentiation and male fertility. Plant Cell 15, 1872-1887.

Supplemental tables

Table 1. Primers used in this study

Primer name	Sequence (5'-3')
Primers for TILLING and mutations confirmation	
DUO1-F1	AACATCAAATTCGAAATGCGAGAGAAAC
DUO1-R1	TCATTCAATCGAATCAGAGTCCAAAGAA
Apk1b-F1	GCTCTTTACTCTCTGATCTCAAAAGGG
Apk1b-R1	CGTTTTGAAATCGCGGTATATGACACTAG
Apk1b-F2	TGTTTCTTGTGGTTGCAGGAG
Apk1b-R2	TGGCTCGTTTACACGACTCATGAA
PKA-F1	ATGGGTTGTGCTTATTCCAAAACTTGCATT
PKA-R1	GTTGATTTTTAGAGTTCCATCCAAAGGTGG
PKA-F2	ACTGAGGAAGATGATGATGGAGAC
PKA-R2	CATTAAGGCGAGTTCACCGAATGA
PKA-F3	ACCTAGGATCTTGCAGCGTTATAC
PKA-R3	GTCATCTGTCCGTTTCATTACCGT
PKA-F4	GAGCGGAATCTGATGAAGAACGTA
PKA-R4	CCTTTTTGAATCAGCCCAAAAAA
EXO70C2-F1	AGAAAGGCGACGTCGTTTCGGATGCT
EXO70C2-R1	ACTTTGTCTCCAGGTTTCCGTCGAGTAGC
EXO70C2-F2	TTGAGAAAGTTAGCATCGACGAGGTGCA
EXO70C2-R2	CTATGTTCTTCGCCTGGCGGTGGC
EXO70H2-F1	AAGAGACTAGAAGACACAAGTGACTCCA
EXO70H2-R1	TCACTAGGAAGAGGTAAGAGAGGGAAAC
EXO70H2-F2	ATTCTTCTAAAGCACTAACTGCAGGAG
EXO70H2-R2	ATGTGCAACAAATAGAAGTGGGCTTACAT
*6-FAM-F	TCGAGGTCGACGGTATCGAT
**VIC-R	TGACGAGTAGACGCTGGTAG

* Sequence was added to the 5' end of the each forward primer.

** Sequence was added to the 5' end of the each reverse primer.

Primers for RNAi

Apk1b RNAi-F	GACCGTTACTTGCTAACAAAAGGAAG
Apk1b RNAi-R	TCAAACAAACAGAGGCGAATCAGAC
PKA RNAi-F	AGAAGATCAAGATGCTCAAAACTGG
PKA RNAi-R	ATGGTCGAAATCATGTTAGACTACGG

Primers for quantitative real time PCR

Apk1b qRT-F	CAGACTCTTACTGCTTCTAAACCG
Apk1b qRT-R	AAACTGCCCCAAGTAATTCACTTC
PKA qRT-F	ATGGGTTGTGCTTATTCCAAAACTTGCA
PKA qRT-R	CCTCTGGACGGAGCTTGTTGATGCG
EXO70C2 qRT-F	AGAACGACAAGGACCCTGATCATGA
EXO70C2 qRT-R	TGGATCTTGATGATCTGTCTCCGCA
Actin 8-F	TGGAACTGGAATGGTTAAGGCTGG
Actin 8-R	TCTCCAGAGTCGAGCACAATACCG

Primers for EXO70C2 T-DNA

EXO70C2 LB	AGTTTTGGTGCAGCATCATTC
EXO70C2 RB	TGGACAGTACTTGGATCCTGG
LB 1.3	ATTTTGCCGATTTCGGAAC

Primers for GUS assay

EXO70C2 GUS-F	GGCTCCTTTGTCTGAACATTTATTTTAG
EXO70C2 GUS-R	GGTTTCTTATTATTTACGTAAAAAGCTT

Primers for subcellular localization

EXO70C2 sub-F1	ATGGAGAAGAACGACAAGGACCC
EXO70C2 sub-R1	CTATGTTCTTCGCCTGGCGGTGG
PEP3 sub-F1	ATGGCGGGTCGGAACATAGAGAAG
PEP3 sub-R1	TTAACCGGTGTTTTGCAATCCTGCAG
H3 sub-F1	ATGGCACGTACGAAGCAAACTG
H3 sub-R1	TCAAGCACGTTCCCCACGAATGC

Table 2: Detailed analysis of mutations found in the *EXO70H2* gene fragment

No	Position from ATG	Exon/ Intron	Amino acid change	Homo/ Hetero	Mutation type
1	G 245 A	Exon	R 82 K	Hetero	Missense
2	C 253 T	Exon	R 86 C	Homo	Missense
3	G 293 A	Exon	H 98 P	Hetero	Missense
4	G 389 A	Exon	R 131 Q	Homo	Missense
5	C 470 T	Exon	S 157 F	Hetero	Missense
6	G 601 A	Exon	E 201 K	Homo	Missense
7	C 717 T	Exon	-	Hetero	Sense
8	C 721 T	Exon	H 241 Y	Homo	Missense
9	C 775 T	Exon	R 259 C	Homo	Missense
10	G 776 A	Exon	R 259 H	Hetero	Missense
11	G 802 A	Exon	V 268 I	Hetero	Missense
12	G 827 A	Exon	R 276 K	Homo	Missense
13	C 987 T	Exon	-	Hetero	Sense
14	G 1145 A	Exon	R 382 K	Hetero	Missense
15	C 1196 T	Exon	S 399 L	Hetero	Missense
16	C 1234 T	Exon	R 412 C	Homo	Missense
17	G 1270 A	Exon	E 424K	Hetero	Missense
18	G 1342 A	Exon	D 448 N	Hetero	Missense
19	C 1386 T	Exon	-	Hetero	Sense
20	C 1450 T	Exon	L 484 F	Hetero	Missense
21	G 1490 A	Exon	R 497 K	Hetero	Missense
22	G 1710 A	Exon	-	Hetero	Sense
23	G 1720 A	Exon	E 574 K	Hetero	Missense
24	G 1803 A	Exon	-	Homo	Sense

25	G 1815 A	Exon	-	Homo	Sense
26	C 1868 T	Exon	S 623 F	Hetero	Missense
27	G 1872 A	Exon	-	Hetero	Sense
28	G 1887 A	Exon	C 629 Y	Homo	Missense